Title

Early transition metal Cu-based single-atom alloys for selective propane dehydrogenation to propylene

Journal

Chem Catalysis, 6(5)

ISSN

2667-1107

Authors

Ngan, Hio Tong
Sautet, Philippe

Publication Date

2026-05-01

DOI

10.1016/j.checat.2026.101691

Cu-Based Single Atom Alloys as Tunable Catalysts for Selective Propane Dehydrogenation

Hio Tong Ngan[1], Philippe Sautet[1,2,3*]

[1]Department of Chemical and Biomolecular Engineering, University of California, Los Angeles, California 90095, United States

[2]Department of Chemistry and Biochemistry, University of California, Los Angeles, California 90095, United States

[3]California NanoSystems Institute, University of California, Los Angeles, CA 90095, United States

Corresponding author: sautet@ucla.edu

Abstract

Propane dehydrogenation is a major reaction in industry as it transforms the abundant propane into propylene, which is a vital raw material for higher-value products. Although Pt-based catalysts have been extensively used for this catalytic process, challenges such as over-dehydrogenation, cracking and coking often pose obstacles to their effectiveness. Here, we utilize first-principles simulations to investigate the potential of Cu-based single-atom alloys (SAAs) as a promising class of catalytic materials for enhancing the reactivity and selectivity for propylene formation. Previously studied SAAs for this reaction are formed by dispersing late and noble transitions metals such as Pt and Rh in Cu. Here we show from first-principles calculations that SAAs formed by dispersing more electropositive, earlier, transition metals such as Ir and even Hf, Ti and Zr into Cu(111) could potentially result in highly efficient catalysts. $CuIr_1$ is demonstrated to possess comparable reactivity to pure Pt and the previously identified $CuRh_1$ catalysts. Additionally, it does not catalyze over-dehydrogenation beyond propylene, as this process is hindered by a large activation barrier. A high propylene production rate, exceeding that on the monometallic Pt catalysts by an order of magnitude, is predicted on $CuHf_1$. Although over-dehydrogenation could take place on $CuHf_1$, which partially covers the catalyst surface with CH_2CHCH_2, further dehydrogenation beyond this intermediate is very unlikely. Chemical bonding analysis demonstrates that the anti-bonding orbitals between Hf and the two atoms (C and H) participating in the first bond-cleavage step of propane is mostly depleted, which leads to the strong interaction between this rate-limiting transition state and the active dopant, and results in the high propylene production rate observed. This strategy of shifting these anti-bonding orbitals above the Fermi level through the introduction of various early-transition metal active elements into the copper substrate may similarly be employed in the engineering of alternative alloy catalysts for catalyzing propane dehydrogenation.

Introduction

Thanks to the breakthroughs in hydraulic fracturing technology, the extraction of shale gas condensates, which are abundant in propane, has seen a remarkable surge in scale.[1] Instead of burning the large amount of propane directly as a fuel, propane can be transformed into more value-added products like propylene. Propylene serves as a vital raw material in the production of crucial petrochemicals including polypropylene, propylene oxide, and acrylonitrile.[2–4] A large portion of the world's production of propylene currently relies on the conventional processes of pyrolysis and catalytic cracking of hydrocarbons. However, due to the swift depletion of fossil fuel resources, these conventional methods utilized for propylene generation are unable to satisfy the rising demands.[1,5] As a result, there is a pressing need to improve the propylene production technologies such that the generation rates could be enhanced.

Non-oxidative dehydrogenation of propane has drawn much attention lately as not only does it generate propylene, but it also yields H_2 which can be used as a clean energy source. In addition, the process is carbon neural. Pt-based catalysts have been widely used in the industry for this dehydrogenation reaction due to their high activity.[6,7] However, over-dehydrogenation and C-C bond cleavage frequently occur on the Pt-based catalysts under reaction conditions, resulting in diminished product selectivity as well as coking.[1,8] Besides, elevated temperatures during alkane dehydrogenation and regeneration processes often lead to significant sintering of Pt nanoparticles, primarily driven by the Ostwald ripening mechanism.[9–11] Furthermore, Pt also imposes an economical constraint on industry profitability due to its expensive cost. These drawbacks necessitate the development of novel catalysts that could offer significant improvements from both a scientific and economic standpoint.

Single-atom alloys (SAA) are a promising class of catalytic materials to improve reaction selectivity and to reduce costs in chemical processes.[12,13] SAAs are often formed by atomically dispersing an active element, such as Pd and Pt, into a less active metal host, such as Cu, Ag, and Au.[14–18] The active elements can initiate the reaction mechanism, which is C-H bond cleavage in the case of propane dehydrogenation, while the less active metal host imparts the selectivity by isolating the active metal and modifying its electronic structure compared to the bulk case. Through diluting different active species in a metal host, the binding strength of reaction intermediates on the surface could be effectively adjusted, which could lead to a control of the reaction kinetics.[19] Depending on how much of the active species is incorporated, remaining in the dilute limit, the resulting active ensembles formed could span various sizes (monomer, dimer, trimer, etc.).[20] These different ensemble sizes dictate the number of active atoms that the reaction intermediates can interact with, and hence determine the binding strength. Small ensemble sizes are also important to limit side reactions of C-C bond formation and coking, since larger active elements are usually required for these coupling reactions.[21] In addition to the geometric contribution, isolated dopant atoms are also expected to have narrow d-states due to the weak orbital mixing between them and the metal host. The relative position of the d-states could also vary when different elements are dispersed in the less active metals.[22] This change in the electronic structures could hence effectively alter the interaction between the catalyst surfaces and the reaction intermediates. By carefully adjusting these two aspects of dilute alloys (i.e. geometric and electronic structures), an optimal catalyst could be achieved, striking a balance between reaction activity and selectivity.

Propane dehydrogenation is a highly endothermic reaction, with a standard enthalpy change of +124.3 kJ/mol.[23] Based on the Le Chatelier's principle, high temperatures are required to promote this endothermic process. Although pure Cu(111) is often prone to sintering (which would lead to catalyst deactivation) when the reaction is performed under high temperatures, the inclusion of active dopant elements such as Ni and Rh in it could provide enhanced sintering resistance, in addition to the improved reaction activity.[13,24] Nevertheless, under high reaction temperatures, alloy catalyst surface restructuring such as segregation (dopant atoms diffusing into the subsurface layers) and aggregation (dopant atoms grouping together to form a large surface active ensemble) should still be properly considered for optimal catalytic performance.

Previously, catalysts created by alloying Sn with Pt were shown to possess good selectivity in the reaction of propane dehydrogenation. Researchers proposed that the inclusion of Sn aids in breaking down larger Pt ensembles into smaller clusters, thereby removing the potential sites for coke formation.[25–27] Additionally, the electronic structure of Pt is also modified with the inclusion of Sn, and the electron transferred from Sn to Pt helps encourage the desorption of propylene and reduce the coke formation on the Pt sites.[28,29] Besides the Pt-Sn catalyst, the highly dilute $CuPt_1$ single atom alloy (SAA) catalyst has also been shown to achieve high propane dehydrogenation selectivity and anti-coke ability, which are attributed to the high barriers for C-C bond breaking and deep dehydrogenation of propene.[12] Another Cu-based SAA catalyst, $CuRh_1$, also demonstrates high activity, selectivity, and coke-resistance in the propane dehydrogenation reaction. In the flow-reactor studies performed by Hannagan et al., not only is this catalyst seen to be more stable, but its activity also surpasses that of the Pt catalyst at low temperatures. Despite the sintering of the Cu nanoparticles at higher temperatures, the initial propane dehydrogenation rates on $CuRh_1$ are still comparable to that on Pt-based catalysts.[13]

The SAAs studied to date are based on late and noble dopants in Cu. In the present paper, we aim at exploring from computations the potential of more electropositive, earlier transition metal dopants, and contrasting them with the known late transition metal dopants. Earlier transition metals are chosen as dopants because (1) SAAs tend to exhibit weaker bindings strengths than pure reactive metals[20,30–33] and (2) in propane dehydrogenation, the initial C-H bond cleavage to form propyl often faces a substantial activation barrier, and it is important to lower it for higher reaction rates.[34] Earlier transition metals, which have higher d-band centers, are hence selected as they are expected to interact sufficiently strongly with the transition state for propane activation, thereby lowering the activation barrier even after accounting for the weakened binding characteristics of SAAs. In this work, we have utilized density functional theory (DFT) calculations and microkinetic modeling to unravel the underlying mechanisms that govern the propane dehydrogenation reaction on four different catalysts: $CuHf_1$, $CuTi_1$, $CuZr_1$, and $CuIr_1$, and compare them with the known $CuRh_1$ and the reference Pt catalysts. By performing a degree of rate control analysis, we show that the rate-limiting step in the dehydrogenation is the first C-H bond cleavage on the early-transition metals in Cu(111) and the Pt catalyst, but that in contrast it is the H-migration from one active dopant to another on $CuIr_1$ and $CuRh_1$. Among the alloy catalysts, the most reactive ones are found to be the early-transition metals in Cu(111) (i.e. $CuTi_1$, $CuZr_1$, and $CuHf_1$) due to their strongest binding with the reaction intermediates and the transition states, leading to a lower effective barrier for C-H bond cleavage. In fact, $CuHf_1$ is calculated to be even more reactive than the conventional Pt catalyst on a per active site basis, and the same should also apply to other early-transition metals in Cu. Besides its reactivity, $CuHf_1$ also possesses high selectivity as further dehydrogenation/decomposition beyond CH_2CHCH_2 is not very likely.

Following $CuHf_1$, $CuIr_1$ and $CuRh_1$ are also found to be active and selective for propane dehydrogenation, despite showing a lower propylene formation rate than $CuHf_1$. Not only do our results demonstrate the potential of SAAs with early transition metal dopants for propane dehydrogenation, but they also illustrate the role of the active dopant in decreasing the destabilizing electronic interaction between the dissociating C-H bond and the metallic active site.

Methods

DFT Calculations. All density functional theory (DFT) calculations were performed using the Vienna ab initio simulation package (VASP).[35,36] Cu-based SAA surfaces for propane dehydrogenation were modeled using a four-layer slab and a (4 × 3) unit cell, with one of the surface Cu atoms replaced by a dopant atom. For this unit cell size, a Γ-centered 4 × 5 × 1 K-points grid was used. During structural optimization, the bottom two layers were fixed in the Cu bulk position while the upper two layers and the surface adsorbates were allowed to relax until the convergence threshold of 0.02 eV/Å was reached. Multiple adsorption configurations of surface species were tested, and the ones that are not used in our discussion are shown in Figures S14 – S17 for reference. Based on the previous benchmarking on Pt(111), the exchange-correlation functional optPBE-vdW is shown to give the most accurate binding energies for alkane activation.[37] Hence, all calculations reported in this study were performed using the optPBE-vdW functional, along with a cutoff energy of 500 eV for the plane wave basis set.[38–40] Transition states were located using the climbing image nudged elastic band method (CI-NEB), the dimer method, and the quasi-Newton method.[41–44] Vibrational frequency calculations were also carried out. Extra imaginary frequencies can occur in minima and transition states due to soft modes associated with alkyl groups. Although these extra imaginary frequencies can in principle be removed by displacement along the associated mode and reoptimization, they are small (the largest one is 77i cm^{-1}) and our tests show that their removal changes the energy in an non-significant manner (by ca. 0.003 eV only). For the free energy calculations, small wavenumbers (< 50 cm^{-1}) and extra imaginary frequencies were shifted to 50 cm^{-1}, and vibrational degrees of freedom were included in the harmonic approximation. Crystal Orbital Hamilton Populations (COHP) analysis was conducted using Local Orbital Basis Suite Toward Electronic Structure Reconstruction (LOBSTER), and all structural configurations reported were visualized using VESTA.[45,46]

Free energy calculations for gaseous and surface species take into consideration zero-point energies and vibrational entropies. They were calculated using equations 1 and 2, respectively:

$$G_{gas,linear} = E_{DFT} + E_{ZPE} + 3.5k_BT + \sum \frac{\epsilon_i}{exp\left(\frac{\epsilon_i}{k_BT}\right)-1} - T\left(S_{trans} + S_{rot} + S_{vib} - k_B ln\frac{P}{P_o}\right) - (1a)$$

$$G_{gas,nonlinear} = E_{DFT} + E_{ZPE} + 4k_BT + \sum \frac{\epsilon_i}{exp\left(\frac{\epsilon_i}{k_BT}\right)-1} - T\left(S_{trans} + S_{rot} + S_{vib} - k_B ln\frac{P}{P_o}\right) - (1b)$$

$$G_{surf} = E_{DFT} + E_{ZPE} + \sum \frac{\epsilon_i}{exp\left(\frac{\epsilon_i}{k_BT}\right)-1} - TS_{vib} - (2)$$

where E_{DFT} is the electronic energy given by DFT, E_{ZPE} is the zero-point energy, ϵ_i is the vibrational energy, k_B is the Boltzmann's constant, T is the temperature, P is the pressure (P_o is the reference pressure), and S_{trans}, S_{rot}, and S_{vib} are the translational, rotational, and vibrational entropies, respectively.

An energy decomposition scheme was employed to understand the stabilization of the transition states for first C-H bond cleavages by splitting the binding strengths into two contributions: transition state deformation and catalyst-transition state interaction.[47] The deformation energy (Eq. 3) for the former and interaction energy (Eq. 4) for the latter were calculated as:

$$E_{def,TS} = E(TS') - E(C_3H_{8,g}) - (3)$$

$$E_{int,TS} = |E(TS - CuX_1) - E(TS') - E(CuX_1')| - (4)$$

where E(TS') is the energy of propane in the deformed geometry of the transition state in the gas phase, $E(C_3H_8,g)$ is the energy of the unconstrained propane molecule in the gas phase, E(TS – CuX_1) is the total energy of the unconstrained transition state on the catalyst surface, and E(CuX_1') is the energy of the frozen metal slab in the deformed geometry of the transition state "TS – CuX_1".

Microkinetic Simulations. Microkinetic simulations were performed to study the kinetic behavior of the proposed reaction mechanism (see SI. Section 2) on the metal catalysts using the energetics obtained from DFT. The rate constants for adsorption ($k_{ads,i}$) and desorption ($k_{des,i}$) were calculated using the collision theory (Eq. 5a and 5b) and those for surface reactions (k_j) using the transition state theory (Eq. 6):[48]

$$k_{ads,i} = \frac{A_{st}}{\sqrt{2\pi m_i k_B T}} - (5a)$$

$$k_{des,i} = k_{ads,i} P^o exp\left(\frac{\Delta G^o_{ads,i}}{k_B T}\right) - (5b)$$

$$k_j = \frac{k_B T}{h} exp\left(-\frac{\Delta H^{\ddagger}}{k_B T}\right) exp\left(\frac{\Delta S^{\ddagger}}{k_B}\right) - (6)$$

where A_{st} is the area of the adsorption site, m_i is the mass of the adsorbing species i, k_B is the Boltzmann's constant, T is the temperature, P^o is the standard state pressure (1 bar), $\Delta G^o_{ads,i}$ is the adsorption free energy of species i under standard state pressure, h is the Planck's constant, and $\Delta H^{\ddagger}$ and $\Delta S^{\ddagger}$ are respectively the enthalpy and entropy differences between the initial state and the transition state in elementary step j.

In the microkinetic simulations, the time-dependent coverages of surface species i were formulated as a combination of the elementary step rate equations r_j:

$$\frac{d\theta_i}{dt} = \sum_j \nu_{ij} r_j - (7)$$

where θ_i is the coverage of surface species i, ν_{ij} is the stoichiometric coefficient of species i in elementary step j, and r_j is the rate equation for elementary step j. The catalyst surfaces were set to be bare initially. Steady-state coverages of surface species, which would be used in subsequent kinetic analysis, could be obtained by constructing a Python script to numerically solve the set of ordinary differential equations.

The degree of rate control (DRC) analysis was employed to identify the rate-limiting steps in propane dehydrogenation over the metal catalysts.[49] It is defined as the change in the overall reaction rate with respect to the change in the rate constant for one specific elementary step j, which could be reflected in the free energy of its transition state. Hence, the mathematical representation for DRC calculations is written as:

$$DRC = \left(\frac{\partial \ln (r)}{\partial \left(\frac{-G_j^{0,TS}}{k_B T} \right)} \right)_{G_{k \neq j}^{0,TS}, G^{0,IM}} \quad -(8)$$

where r is the overall reaction rate, and $G^{0,TS}$ and $G^{0,IM}$ are respectively the standard state free energies of the transition states and the surface intermediates.

PDH is usually carried out at T = 500 – 700 °C and atmospheric pressure.[23,50] We selected the lower end of this range, i.e. 500 °C, for this study, a total pressure of 1 bar and a conversion of 15%.[1] A partial pressure of H_2 is often initially mixed with propane reactant to limit coke formation, hence we set 75% propane and 25% H_2 as the initial composition. Considering the 15% conversion, simulations are therefore performed at T = 773 K, P(C_3H_8) = 0.64 bar, P(H_2) = 0.36 bar, and P(C_3H_6) = 0.11 bar.

Results

Table 1. Segregation and aggregation energies of various dopants in Cu(111) in vacuum. Negative segregation energies indicate favorable segregation, while positive aggregation energies signify unfavorable aggregation. Reproduced from ref 19.

Dopant	Segregation Energy	Aggregation Energy
Ti	**0.22 eV**	**0.04 eV**
Zr	**-0.11 eV**	**0.46 eV**
Hf	**0.10 eV**	**0.56 eV**
Ir	**0.04 eV**	**0.05 eV**
Rh	**0.02 eV**	**0.15 eV**

Dopant Segregation and Aggregation. In contrast to monometallic catalysts such as Pt, concern is often raised regarding the position of the active species in single-atom alloy catalysts. Segregation and aggregation energies are two important indicators that assess whether a single-atom alloy catalyst, with active species monomers embedded in the surface layer of the host, could be formed experimentally. The former is defined as the energy gain/loss when the dopant goes from subsurface Cu layer to the surface layer, and the latter is the energy difference when two isolated surface dopant atoms are brought together to form a dimer. Hence, negative segregation energy indicates that it is favorable for the dopants to stay in the surface layer, and positive aggregation energy suggests that the dopants would like to remain isolated. The calculation of segregation and aggregation energies is usually done in vacuum in the literature, while the presence of adsorbates in reaction conditions could markedly affect these values, as we will discuss later.

An earlier study found that, in vacuum, the segregation of active Zr dopant to the Cu(111) surface is energetically favorable, as evidenced by the negative energy value of -0.11 eV for this process (Table 1).[19] In contrast, for $CuTi_1$, $CuHf_1$, and $CuIr_1$, the segregation energy values are positive, ranging from 0.04 to 0.22 eV.[19] While these positive values suggest unfavorable segregation and preference for migration towards the bulk, their magnitudes are relatively small, and this impediment can be alleviated by the presence of adsorbates under reaction conditions. Besides segregation, it is noted that the aggregation energies are positive for all alloy catalysts. The formation of larger dopant aggregates is therefore not thermodynamically favorable, and the

dopants should stay as isolated atoms in the surface layer. Nevertheless, one needs to assess as well the influence of adsorbates on dopant aggregation, as will be discussed in more detail.

To provide some examples, the synthesis of model $CuTi_1$ samples has already been demonstrated to be feasible by Weaver et al. by vapor deposition of Ti on a Cu(111) surface.[51] Another work by Biener et al. synthesized Ti doped nanoporous Cu samples by chemical dealloying of $Al_{80}Cu_{19}Ti_1$ precursor alloys and suggested that isolated Ti atoms in the surface of Cu are the active sites for the H-D exchange reaction observed in their study.[52] Since Hf, Zr, and Ir have smaller segregation energies and larger aggregation energies than Ti, it is very likely that they could be made experimentally as well. One can further underline that the segregation energy for $CuRh_1$ is calculated to be 0.02 eV, hence very similar to that of $CuHf_1$ and $CuIr_1$, while experiments have shown that $CuRh_1$ SAA is both active and stable for propane dehydrogenation.[13] As a result, not only are the chosen SAAs in this work anticipated to be synthesizable in experiments, but they will also remain stable under reaction conditions.[13]

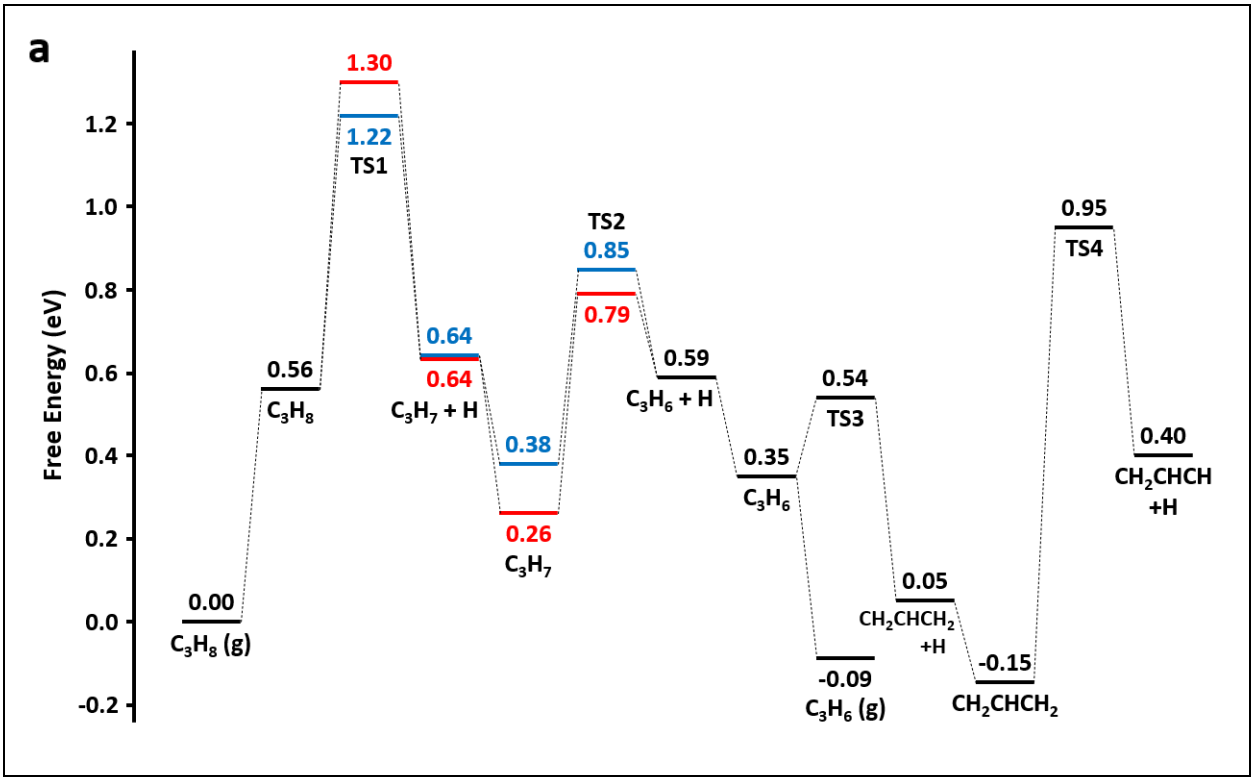

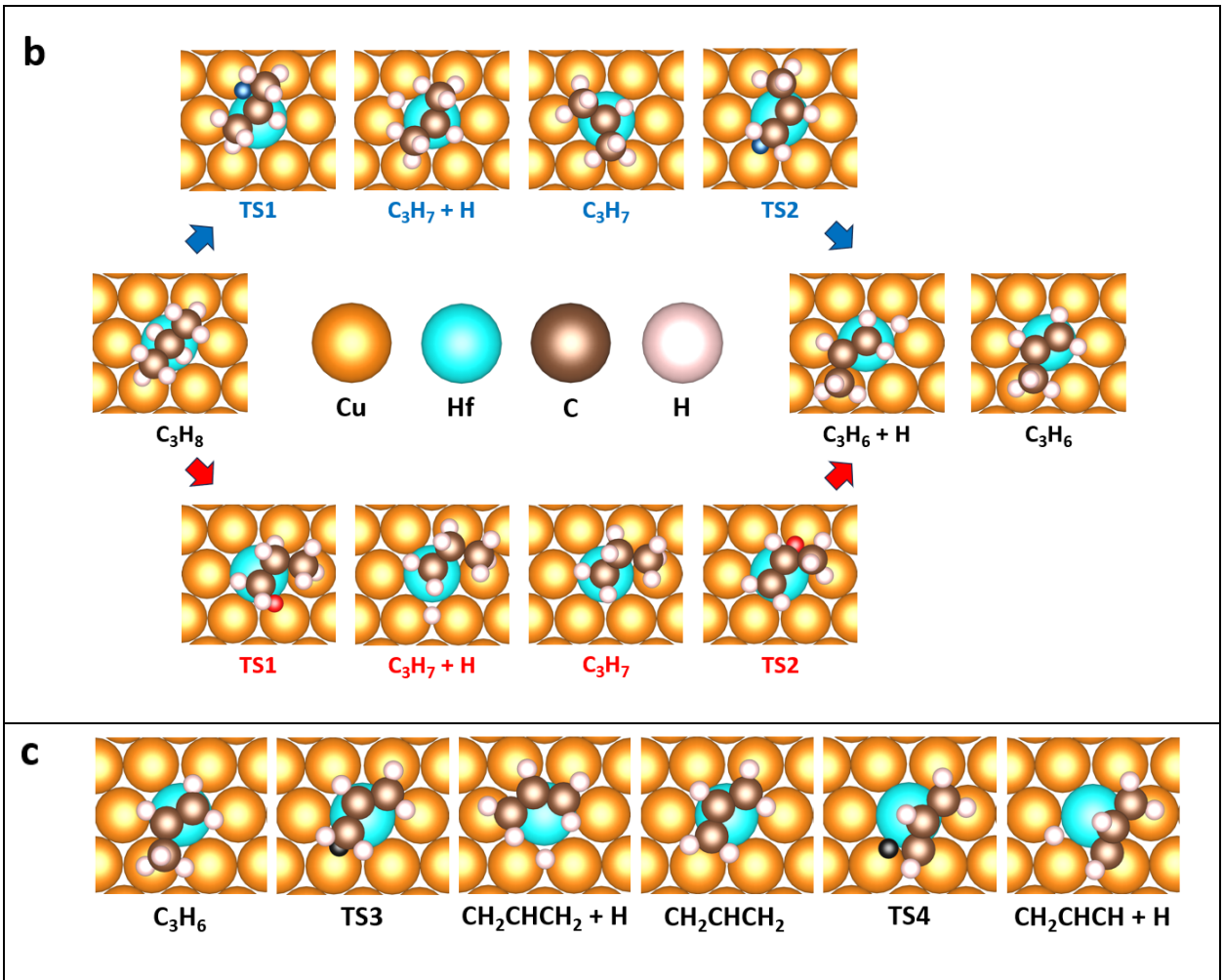

Figure 1. (a) Free energy profile and (b,c) corresponding adsorption configurations for propane dehydrogenation on $CuHf_1$. Side view of the transition states is provided in Figure S1. Red and blue sections along the pathway indicate dehydrogenation at the terminal or central carbon atoms as the first step, respectively. For better visibility, the H atoms that are being detached in the transition states are colored in red or blue, accordingly, and in black for further dehydrogenation beyond propene. Reaction conditions are: T = 773 K, $P(C_3H_8)$ = 0.64 bar, $P(H_2)$ = 0.36 bar, and $P(C_3H_6)$ = 0.11 bar.

Propane Activation. We will first describe the catalytic activity of $CuHf_1$. Propane activation could take place by either cleaving the C-H bond at the terminal carbon atom first (Figure 1, red pathway) or at the central carbon atom first (Figure 1, blue pathway). Free energy profiles for these reaction pathways were constructed for the single-atom alloy catalysts and the monometallic Pt catalyst to examine the differences among them (Figure 1, S8, S10, and S11). On $CuHf_1$, the free energy profile begins with the molecular adsorption of propane (C_3H_8) on the dopant, followed by the transition states for C-H bond cleavage to form either CH_3CHCH_3 (blue pathway) or $CH_3CH_2CH_2$ (red pathway), which co-adsorb on the same active ensemble with the H atom detached ("C_3H_7 + H" in Figure 1). For the presentation of the free energy profile, we assume that, before subsequent bond-breaking steps take place, this H atom will spill over on the Cu domain and recombine with another H atom either on the Cu surface directly or on a second active site,

and effectively desorb as ½ H_2(g). Although these processes (H-spillover and H-H recombination) are activated, they are not included in Figure 1 for simplicity, but they will be detailed in the following section. As will be confirmed by the following sections, this assumption does not affect the conclusion drawn from this free-energy-based analysis for $CuHf_1$. After the H atom is removed, the propyl intermediate will follow the same dehydrogenation pattern to produce C_3H_6. Propylene formed on $CuHf_1$ could either desorb into the gas phase or stay on the surface for further reaction. Further reaction involves cleaving the C-H bond in the methyl group in propylene, generating an allyl intermediate CH_2CHCH_2 on the catalyst surface. Eventually, the resulting CH_2CHCH_2 will undergo additional dehydrogenation and terminate at CH_2CHCH + H. Free energy profiles for $CuIr_1$, $CuRh_1$, and Pt(111) were constructed in a similar manner, although they stop at CH_2CHCH_2, and the reason of which will be discussed in the following section.

The free energy profile for propane dehydrogenation on $CuHf_1$ indicates that molecular adsorption of propane is not stable under the studied conditions, as demonstrated by the positive change in free energy (ΔG = 0.56 eV). Following this molecular adsorption, the transition state to break the C-H bond at the central C atom (blue pathway) is seen to be more favorable than that at the terminal C atom (red pathway), as evidenced by the lower free energy value of 1.22 eV versus 1.30 eV. The fact that these two transition states lie at the highest points in the entire free energy profile suggests that they are the most rate-limiting steps in this reaction. Since the blue pathway is more favorable, the reaction is expected to proceed predominantly along this route and thus exert greater control over the overall reaction rate. Consequently, blue TS1 should be more rate-controlling than red TS1, as will be proved in the following section. In contrast with the energy ranking of the first transition states, the intermediate formed by dehydrogenating the central C atom (blue C_3H_7; G = 0.38 eV) is less stable than that formed by terminal C dehydrogenation (red C_3H_7; G = 0.26 eV). Surprisingly, when the H atom remains co-adsorbed with these propyl intermediates (C_3H_7 + H), they are equally stable. This observation can be attributed to the stronger repulsive interaction between the H atom and the propyl intermediate in the red pathway than in the blue pathway, as demonstrated by the larger structural displacement observed for propyl in the co-adsorbed 'C_3H_7 + H' state along the red pathway. Lastly, the second transition states for C-H bond cleavage to produce the desired product propylene follows the same trend as the propyl intermediates, i.e. red TS1 lies lower in the free energy profile than blue TS1. It is worth noting that although the red pathway is more favorable than the blue pathway in this second bond-breaking step, the transition state energies for these steps are much lower than those for the first ones. Hence, it will not reverse the qualitative statement that the blue pathway is more favorable.

Propylene formed on $CuHf_1$ could either desorb into the gas phase or stay on the catalyst surface for further dehydrogenation. It is seen that the activation barrier for additional C-H bond cleavage is considerably small (0.19 eV). This small activation barrier implies that this further dehydrogenation step to produce CH_2CHCH_2, which is remarkably stable on the catalyst surface (G = -0.15 eV; lower than that of gaseous propylene by 0.06 eV), is indeed very probable. However, dehydrogenation beyond CH_2CHCH_2 is less likely as the forward activation barrier (ΔG = 1.10 eV) is 0.41 eV larger than the reverse barrier to produce propylene again. An alternative dehydrogenation pathway leading to propyne formation was also examined (Figure S2). This pathway is shown to be even less favorable, as the transition states (G = 1.22 – 1.25 eV; relative to C_3H_8(g)) associated with cleavage of the remaining C-H bonds in propylene lie high on the free energy profile, and are even higher than TS3 for CH_2CHCH_2 formation and TS4 for further dehydrogenation. Besides dehydrogenation, CH_2CHCH_2 decomposition to form CH_2CH and CH_2

is also improbable due to the substantial free energy difference ($\Delta G = +0.90$ eV) between the intact (CH_2CHCH_2) and the fragmented ($CH_2CH + CH_2$) states (Figure S3). The presence of the activation barrier associated with C-C bond cleavage would further exacerbate the difficulty of this process. Eventually, since CH_2CHCH_2 is more stable than C_3H_6, $CH_2CHCH + H$, and $CH_2CH + CH_2$, the reaction is expected to be trapped here, populating the catalyst surface with CH_2CHCH_2.

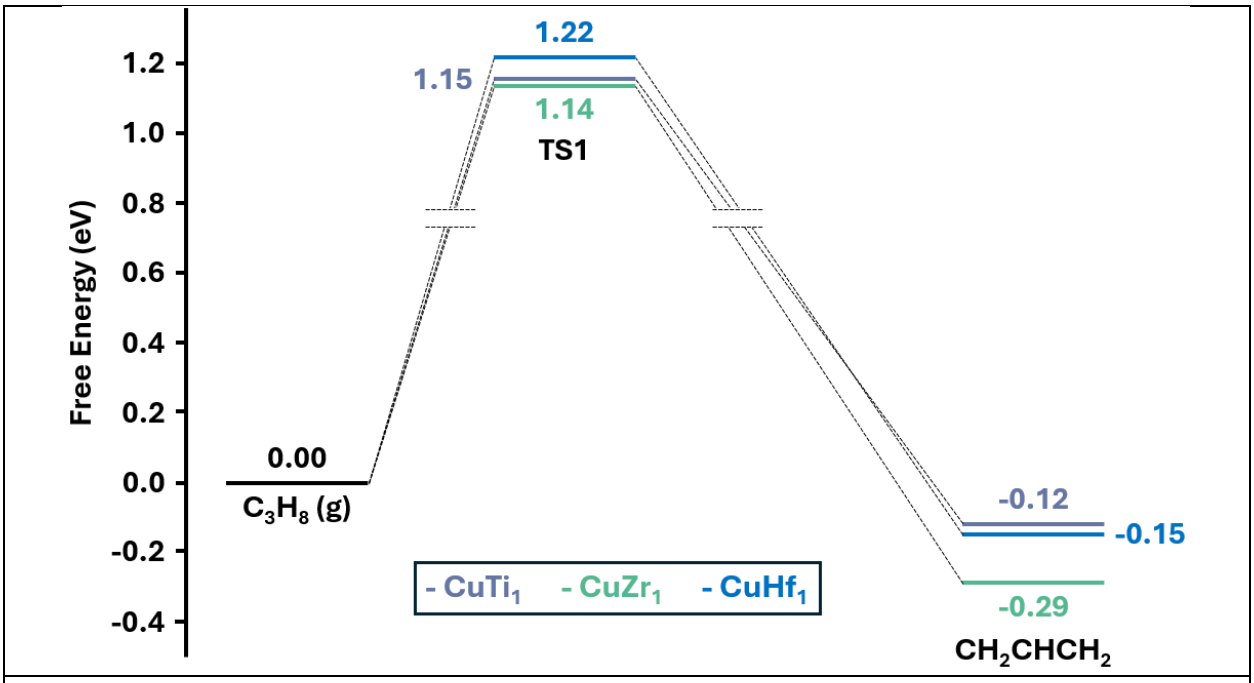

Figure 2. Simplified free energy profile for propane dehydrogenation on $CuTi_1$ (gray), $CuZr_1$ (aquamarine), and $CuHf_1$ (blue). Reaction conditions are T = 773 K, $P(C_3H_8) = 0.64$ bar, $P(H_2) = 0.36$ bar, and $P(C_3H_6) = 0.11$ bar.

As previously mentioned, the rate of propane dehydrogenation is predominantly controlled by the initial activation of the molecule, and the strong adsorption of CH_2CHCH_2 might lead to catalyst poisoning, resulting in lower activity. Based on these claims made for $CuHf_1$, we extended this study to other early-transition metals in Cu(111) and explored their catalytic performance relative to $CuHf_1$ (Figure 2). Similar to $CuHf_1$, $CuTi_1$ and $CuZr_1$ favor the pathway in which the C-H bond at the central carbon atom of propane is cleaved first. Additionally, the free energies associated with the transition states for initial activation (G = 1.14 – 1.22 eV) and CH_2CHCH_2 adsorption (G = -0.29 – -0.12 eV) are similar among the three catalysts, and the catalytic performance of $CuTi_1$, $CuZr_1$, and $CuHf_1$ is hence expected to be comparable. For this reason, the following discussion will primarily focus on the difference between the early- and mid-transition metals in Cu(111), rather than among the three early-transition metals.

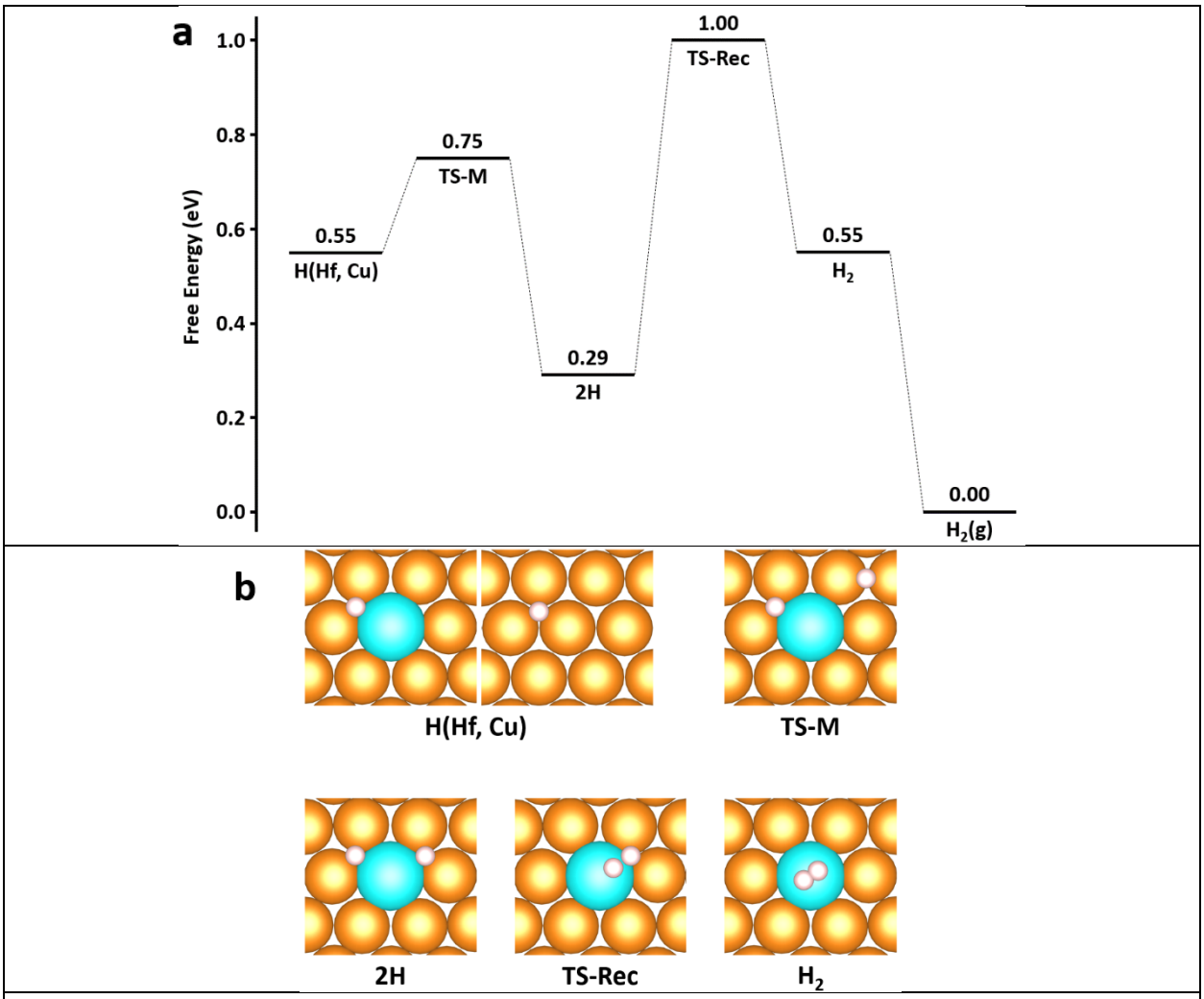

Figure 3. (a) Free energy profile and (b) corresponding adsorption configurations for H atoms recombination on $CuHf_1$. Reaction conditions are: T = 773 K and $P(H_2)$ = 0.36 bar.

H-H Recombination. It is worth noting that, on single-atom alloys, the H atoms detached from propane and propyl will recombine on either a second active site or on Cu(111) before desorbing into the gas phase. The energy profile for such processes on $CuHf_1$ is shown in Figure 3. To achieve the recombination on a second $CuHf_1$ active site, it is needed to bring the H atoms already spilled over on the Cu domain to the single atom by overcoming a small migration barrier of ~ 0.20 eV. The same process was also assessed for the other four alloy catalysts (i.e. $CuTi_1$, $CuZr_1$, $CuIr_1$ and $CuRh_1$), which reveals migration barriers of similar magnitudes to that observed on $CuHf_1$ (Figures S5, S6, S7 and S9). Once there are two H atoms on the same active ensemble ("2H" state in Figure 3, S5, S6, S7 and S9), recombination could take place by going through the associated transition state ("TS-Rec"). In the case of the early-transition metals ($CuTi_1$, $CuZr_1$ and $CuHf_1$), this recombination process is considerably more difficult than that on $CuRh_1$ and $CuIr_1$ for their high transition state energies (G = 0.96 - 1.00 eV) and large activation barriers of 0.70 – 0.77 eV (Figures 3, S5 and S6). For $CuRh_1$, on the other hand, the recombination transition state is at a comparable level to the molecular adsorption state of H_2, making the activation barrier small and roughly equal to 0.1 eV (Figure S9). Lastly, the binding of the H atoms on the $CuIr_1$ active sites is

strong, with the adsorption free energy being -0.02 eV at the high reaction temperature (Figure S7). This binding is so strong that no recombination transition state was found on the electronic energy surface and the two H atoms simply desorb as a gaseous H_2 molecule. Nevertheless, given the entropy change associated with adsorption/desorption processes, there should exist a free energy barrier in between gaseous H_2 and the "2H" state that we assume as negligible here. Before closing up, it should also be mentioned that the only barrier for H-H recombination on Pt(111) is the binding energy of the H atoms,[53] and the transition state energy and activation barrier for the same process on Cu(111) are 1.55 eV and 0.74 eV, respectively. Although these values are larger than those on the active ensembles, Cu(111) could still serve as additional sites in the reaction mechanism to recombine the H atoms from propane activation.

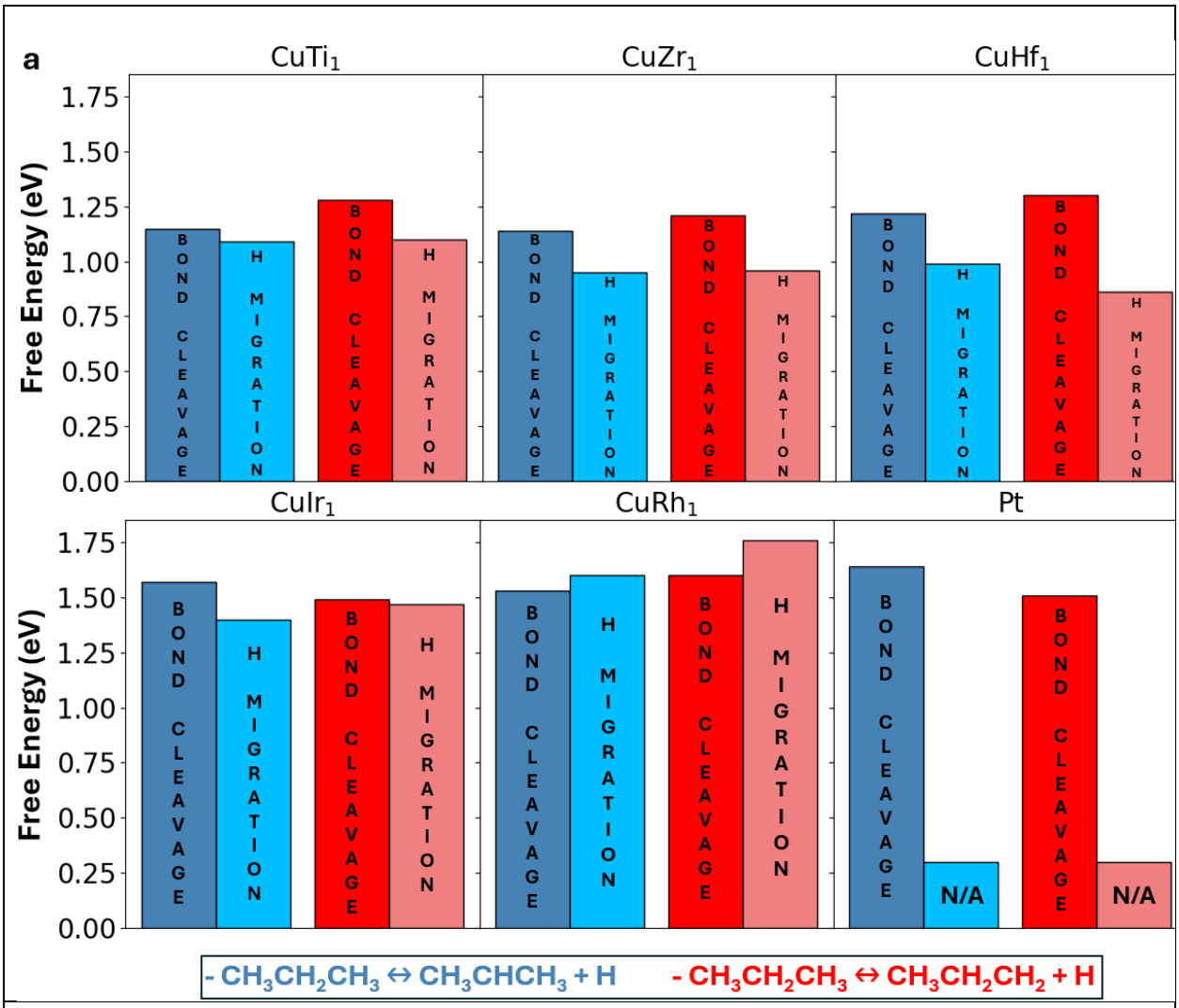
a
CuTi1
CuZr1
CuHf1
CuIr1
CuRh1
Pt
Free Energy (eV)
1.75
1.50
1.25
1.00
0.75
0.50
0.25
0.00
BOND CLEAVAGE
H MIGRATION
N/A
- CH3CH2CH3 ↔ CH3CHCH3 + H
- CH3CH2CH3 ↔ CH3CH2CH2 + H

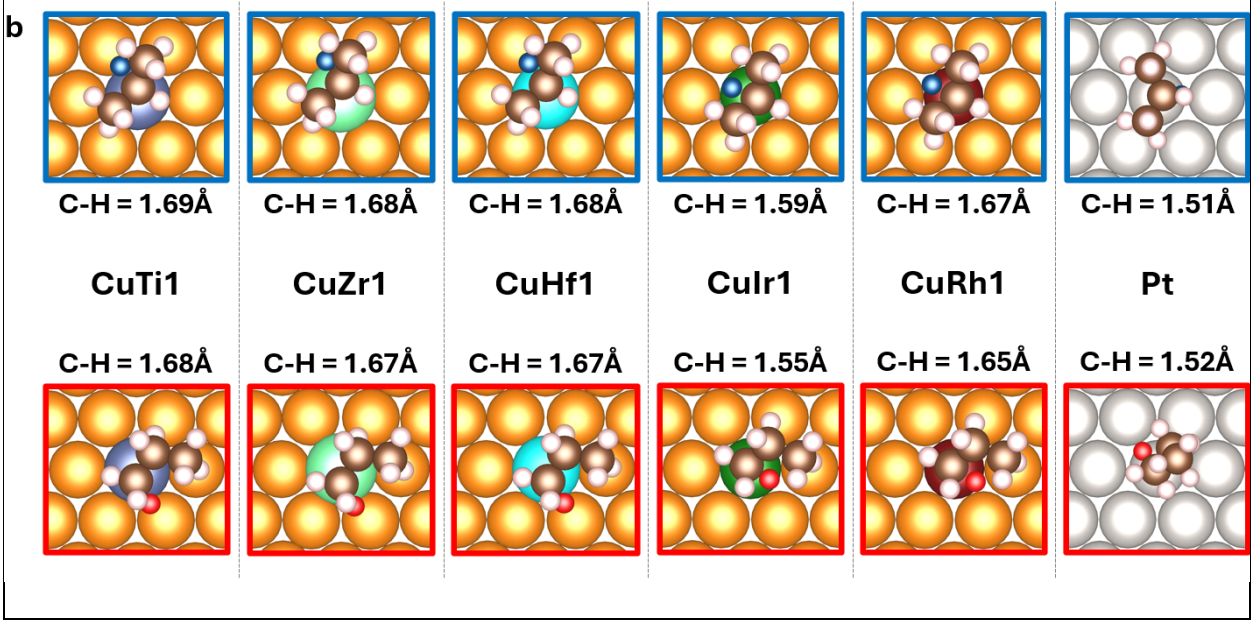
b
C-H = 1.69Å
C-H = 1.68Å
C-H = 1.68Å
C-H = 1.59Å
C-H = 1.67Å
C-H = 1.51Å
CuTi1
CuZr1
CuHf1
CuIr1
CuRh1
Pt
C-H = 1.68Å
C-H = 1.67Å
C-H = 1.67Å
C-H = 1.55Å
C-H = 1.65Å
C-H = 1.52Å

Figure 4. (a) Free energies of the transition states for the steps of initial C-H bond cleavage and subsequent H-migration away from the active ensembles. Note that H-migration steps are not considered for Pt(111) due to the homogeneous nature of the surface. The free energies of the H-migration transition states were obtained by adding the activation barriers, which are the energy differences between "C_3H_7 + TS-M (in the absence of the H residing on the active ensemble)" and "C_3H_7 + H", to "C_3H_7 + H". A schematic diagram for this process is provided in Figure S12. (b) Corresponding adsorption configurations of the transition states for the initial C-H bond cleavage steps on the catalyst surfaces, along with the lengths of the C-H bonds that are being cleaved listed. Side view of these transition states can be found in Figures S1, S8, S10 and S11. Blue and red colors for bars and frames represent the pathways in which the central or terminal carbon atoms of propane are dehydrogenated as the first step, respectively. The H atoms that are being detached are highlighted in blue or red accordingly. Reaction conditions are: T = 773 K, $P(C_3H_8)$ = 0.64 bar, $P(H_2)$ = 0.36 bar, and $P(C_3H_6)$ = 0.11 bar.

Transition State Energy Comparison. The complete propane dehydrogenation pathway was also studied in detail on $CuIr_1$, $CuRh_1$, and Pt(111) (Figures S8, S10 and S11), in addition to $CuHf_1$ (Figure 1). It is determined by the lower overall transition state free energies that $CuRh_1$ exhibits a preference for the production of propylene through CH_3CHCH_3 (i.e. blue pathway), whereas $CuIr_1$ and Pt(111) opt for $CH_3CH_2CH_2$ (i.e. red pathway) for the same process (Figure 4). However, unlike the early-transition metals in Cu(111) (i.e. $CuZr_1$, and $CuHf_1$; for $CuTi_1$, propane activation appears to be the sole rate-limiting step as well, although this conclusion should be interpreted with caution given the small difference of 0.06 eV between the bond cleavage and H-migration transition state energies in the blue pathway), propane activation is not the sole rate-limiting step on $CuIr_1$ and $CuRh_1$. For $CuIr_1$, the first C-H bond cleavage transition state in the red pathway is only 0.02 eV higher in free energy than the H-migration step towards the Cu domain (Figure 4). For $CuRh_1$, the transition state for the spillover step in the blue pathway lies even higher in the energy profile than the bond cleavage step (Figure 4). These results strongly indicate that H-migration steps are also rate-controlling in the reaction mechanisms on these two single-atom alloys, which stand in stark contrast to the prevailing belief that alkane activation is only governed by the initial bond-cleavage step. It is noteworthy that the change in the rate-limiting steps is most likely attributed to the stabilization of the dehydrogenated intermediates (i.e. "CH_3CHCH_3 + H" and "$CH_3CH_2CH_2$ + H"). To be more specific, on $CuHf_1$, the intermediate is stabilized (relative to the first bond cleavage transition state) to a greater extent than that on $CuIr_1$ and $CuRh_1$, as evidenced by the free energy differences between the first bond cleavage transition states and the intermediate states (ΔG = -0.58 eV for $CuHf_1$, ΔG = -0.37 eV for $CuIr_1$, and ΔG = -0.28 eV for $CuRh_1$). Additionally, the three alloy catalysts encounter similar activation barriers for the H-migration steps ($\Delta G^{\ddagger}$ = 0.35 – 0.40 eV; note that these barriers are lower when reaction intermediates are present due to repulsion, as opposed to situations where only one H atom is present or no species are present at all). These two aspects collectively lead to higher transition state energies for H-migration on $CuIr_1$ and $CuRh_1$, consequently rendering this event somewhat rate-controlling in the reaction network. To avoid proceeding through the rate-limiting H-migration steps, it might be possible to keep the H atoms on the active ensembles while cleaving the second C-H bonds in propyl. However, the transition states for these steps on $CuIr_1$ and $CuRh_1$ are demonstrated to possess even higher free energies than those for H-migration (> 0.11 eV), suggesting that this pathway is less favorable and is not considered in this study (Figure S13). In

comparison, on the Pt(111) catalyst, H diffusion is easy and H-migration steps cannot govern the dehydrogenation rate.

In addition to the distinct rate-limiting steps, the highest transition state free energies for the more preferrable pathway on $CuIr_1$, $CuRh_1$, and Pt(111) markedly exceed those observed for the early-transition metals (Figure 4). To clarify further, the free energy values range from 1.49 – 1.60 eV for the former, versus 1.14 - 1.22 eV for the latter. These larger values could indicate that the corresponding reaction rates would be significantly lower when compared with $CuTi_1$, $CuZr_1$, and $CuHf_1$. Nevertheless, $CuIr_1$ and $CuRh_1$ encourage propylene desorption by imposing large activation barriers (Figures S8 and S10; $\Delta G^{\ddagger} = 1.13$ eV for $CuIr_1$ and $\Delta G^{\ddagger} = 0.89$ eV for $CuRh_1$) for further dehydrogenation steps. Even if this additional bond cleavage step can take place, the resulting CH_2CHCH_2 formed is not strongly bound, as indicated by the positive free energy changes of 0.46 – 0.50 eV for this intermediate state relative to gaseous propylene. Hence, propylene is not expected to undergo more dehydrogenation steps and these catalyst surfaces should not be populated by the intermediate CH_2CHCH_2. It is not straightforward from the pathways alone to decipher whether the activation barrier magnitude or the surface poisoning by intermediates will control the optimal propylene production rates on these SAA catalysts. The combined effect of these contributions will be thoroughly examined in the following microkinetic modeling section.

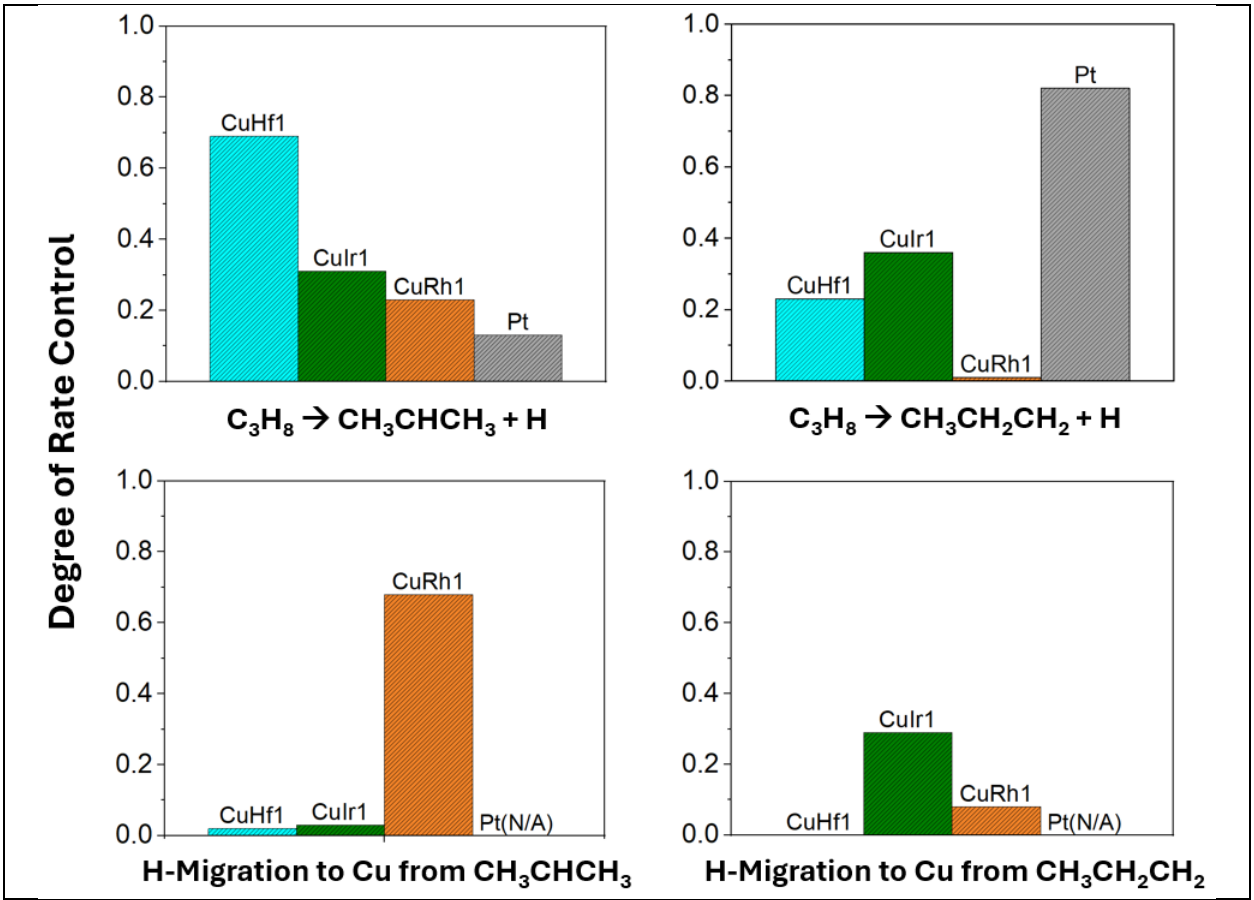

Figure 5. Degree of rate control of the transition states for the steps of initial C-H bond cleavage and subsequent H-migration away from the active ensembles. Note that H-migration steps are

not considered for Pt(111) due to the homogeneous nature of the surface. Reaction conditions are: T = 773 K, $P(C_3H_8)$ = 0.64 bar, $P(H_2)$ = 0.36 bar, and $P(C_3H_6)$ = 0.11 bar.

Microkinetic Simulation of Catalytic Activity and Selectivity. Microkinetic modeling was performed to assess the combined effect of intermediate free energies and transition state free energies on the reaction rate. It also brings the two separate pathways of propane activation and H-H recombination together to provide a more comprehensive analysis of the activity of SAA catalysts. The details of the elementary steps considered in the reaction network can be found in Supplementary Information (Tables S1-S4). Briefly, the elementary steps include propane activation and dehydrogenation on the SAA surface (Propane Activation Section), and H-H migration and recombination on both the Cu(111) and SAA surfaces (H-H Recombination Section). Microkinetic modeling indicates that on $CuHf_1$, the transition states for dehydrogenating the central and terminal C atoms of propane are the most rate-controlling (Figure 5). Although both dehydrogenation pathways demonstrate a certain degree of rate control (i.e. reaction takes place through both pathways), the fact that dehydrogenating the central C atom of propane is more rate-controlling supports the free-energy-based analysis, where this pathway was shown to be more favorable and of primary importance. Similarly, reaction proceeds via both dehydrogenation pathways on $CuIr_1$, as evidenced by the degree of rate control exhibited by them. In this case, however, the pathway of dehydrogenating the terminal C atom of propane as an initial step is shown to be more favorable by the greater degree of rate control. More importantly, C-H bond cleavages are not the sole rate-limiting steps in alkane activation on $CuIr_1$. Rather, the step of moving the H atom away from $CH_3CH_2CH_2$ also significantly controls the reaction rates. This situation starkly contrasts with extended active surfaces, on which the breaking of the C-H bonds is believed to be the only limiting factor for reaction rates. It is noted that the step of H-migration becomes even more prominent on $CuRh_1$, as this transition state is the most rate-limiting in the reaction network, more rate-limiting than those for C-H bond cleavage (Figure 5). This observation is consistent with the free-energy-based assessment, where the free energy of this transition state is higher than that for dehydrogenating the central C atom of propane in the more favorable pathway (Figure 4). Eventually, the larger DRC value of the transition state for dehydrogenating the terminal C atom of propane on Pt(111) agrees well with the previous analysis that the reaction primarily proceeds through this pathway (Figures 4 and 5). Unlike the single-atom alloy catalysts, H-migration does not play a significant role in controlling the reaction rates on Pt(111) due to the homogeneous nature of the catalyst surface.

Before proceeding further, it is necessary to discuss the H-migration step being rate-limiting in more detail. As shown in Figures S8 and S10, mid-transition metals (Ir and Rh), as a SAA in Cu, do not interact strongly with propyl, hence placing the states of 'C_3H_7 + H' and 'C_3H_7' high in the free energy profiles. Migrating H atoms away from the active ensembles is an activated process, meaning there is an associated transition state and activation barrier. Since the initial state (C_3H_7 + H) already lies high in the free energy profile, the transition state corresponding to H-migration would lie even higher on the same profile. Accordingly, the H-migration steps would become rate-limiting as long as their transition states are comparable in energy to TS1. This phenomenon applies to mid-transition metals (i.e. Ir and Rh) and is also likely relevant for late transition metals on Cu(111), but not for the early-transition metals (i.e. Hf), which are known to bind strongly to hydrocarbons. These findings collectively suggest that in future research endeavors regarding

alkane activation on single-atom alloys, attention should also be directed to H-migration, in addition to the ease of C-H bond activation.

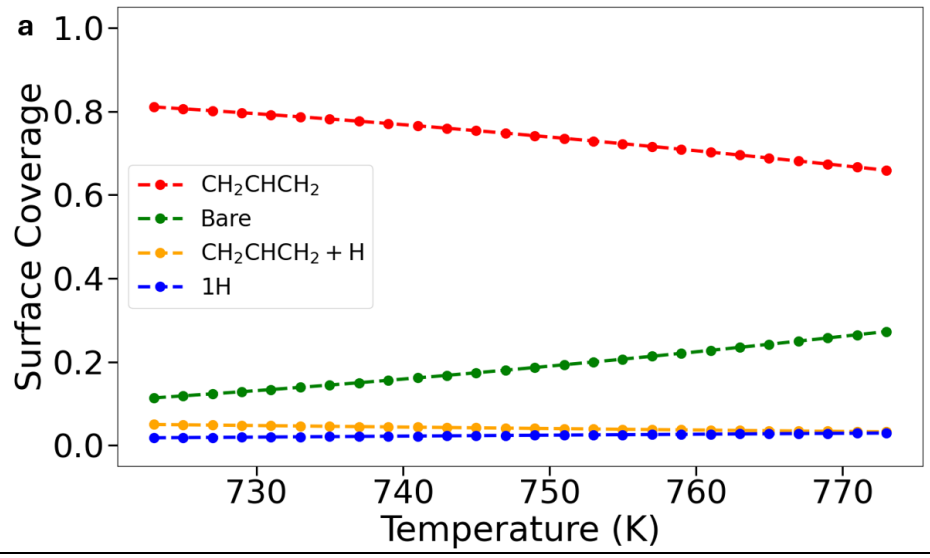

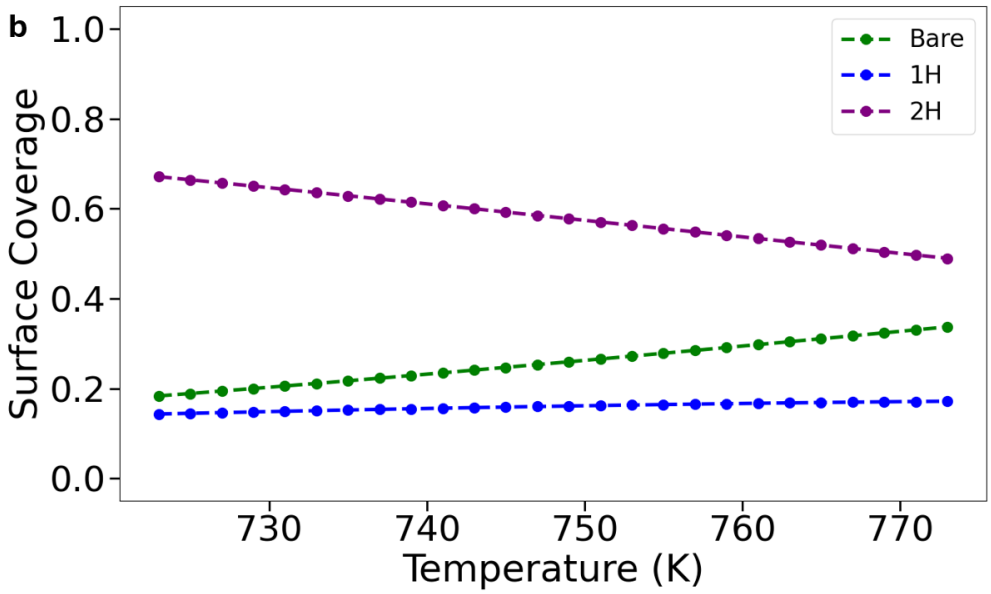

Figure 6. Steady-state surface coverage of reaction intermediates on (a) $CuHf_1$ and (b) $CuIr_1$ as a function of temperature. Reaction conditions are: $P(C_3H_8)$ = 0.64 bar, $P(H_2)$ = 0.36 bar, and $P(C_3H_6)$ = 0.11 bar.

The catalyst surfaces could be populated by reactants and intermediates during the course of the dehydrogenation reaction, which could lead to surface poisoning and catalyst deactivation. Results of kinetic modeling show that on $CuHf_1$, most of the active sites are covered by CH_2CHCH_2 due to its strong binding on the surface (Figures 1 and 6a; G = -0.15 eV), with the coverage being ~80 % at lower temperature and ~65 % at higher temperature. Despite this partial blocking of the active

ensembles by the strongly bound CH_2CHCH_2 intermediate, there are still some vacant sites (approximately 12 % to 28 %) available for reactions. Given that the free energies of the transition states for propane activation are considerably lower on $CuHf_1$, it is expected that this catalyst could still efficiently produce propylene with only a fraction of active sites accessible. Unlike $CuHf_1$, it is the H atoms (Figure 6b) that populate the surface of $CuIr_1$, for their strong adsorption on the active ensembles (Figure S7; G = -0.02 eV for the "2H" state). The coverage of these H atoms ("1H" and "2H") accounts for ~65 % to 80 % of the total active sites, leaving only 20 – 35% of the sites bare for dehydrogenation. Although the amount of vacant active sites is similar on both $CuHf_1$ and $CuIr_1$, propylene production rate should be lower on the latter due to the higher transition state free energy associated with the first C-H bond cleavage step. Eventually, it is seen that the surface of $CuRh_1$ is mostly bare (Figure S18), as there is no strongly bound reaction intermediate on it.

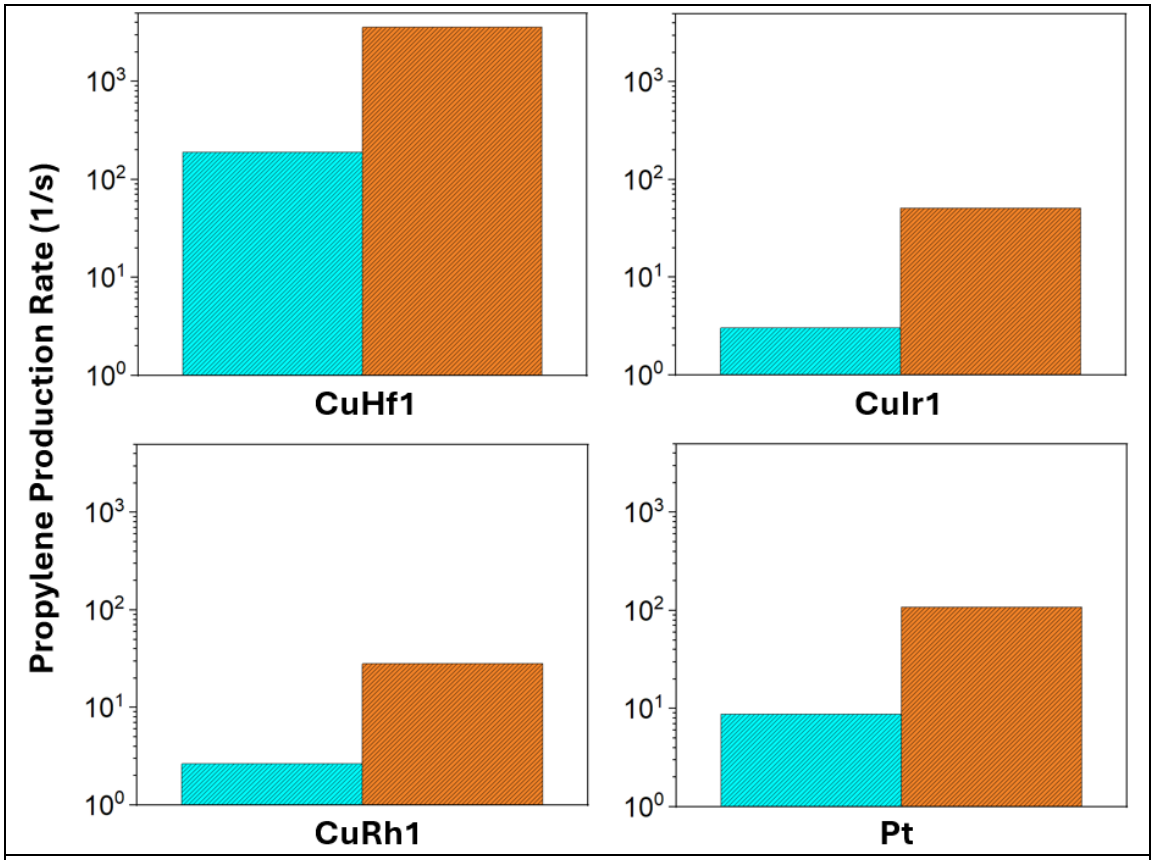

Figure 7. Steady-state rate of propylene production on the four catalyst surfaces. Blue represents the production rate at a lower temperature of 723 K and brown is at a higher temperature of 773 K. Pressures of reactants and products are: $P(C_3H_8)$ = 0.64 bar, $P(H_2)$ = 0.36 bar, and $P(C_3H_6)$ = 0.11 bar.

The rate of propylene production reflects the result of the interplay between activation barriers and surface poisoning. It is seen that $CuHf_1$ is the most reactive catalyst (191 s^{-1} at T = 723 K; 3576 s^{-1} at T = 773 K) among the four for propylene production (Figure 7), although only a small portion of its active sites are available for dehydrogenation. More importantly, this single-atom alloy catalyst is markedly more reactive than Pt(111) (8.8 s^{-1} at T = 723 K; 108 s^{-1} at T = 773 K) on a

per active site basis, which suggests its potential to replace the currently-used Pt-based catalysts. It is worth noting that other early transition metals in Cu(111) (i.e. $CuTi_1$ and $CuZr_1$) should also possess similar propylene production rates to $CuHf_1$ due to the comparable transition state free energies for propane activation and adsorption free energies of CH_2CHCH_2 as seen earlier (Figure 2). $CuIr_1$ and $CuRh_1$, on the other hand, demonstrate propylene formation rates resembling that of Pt(111) (2.6 s^{-1} at T = 723 K and 28.2 s^{-1} at T = 773 K for $CuRh_1$; 3.0 s^{-1} at T = 723 K and 50.9 s^{-1} at T = 773 K for $CuIr_1$), which are significantly lower than that observed on $CuHf_1$. These lower reaction rates are aligned with the higher transition state free energies as observed in Figure 4.

Single-atom alloy catalysts offer many advantages that conventional monometallic catalysts (e.g. Pt) do not possess. For example, the inherent geometric constraint (i.e. small ensemble size) of single-atom alloys prevents them from engaging in unwanted side reactions such as C-C bond breaking and deep-dehydrogenation, which would typically occur on extended active surfaces.[1,8] Such side reactions could lead to diverse serious issues, including carbon coking and subsequent catalyst deactivation. Even though propylene dehydrogenation could take place on $CuHf_1$, the resulting CH_2CHCH_2 intermediate cannot proceed further to form either CH_2CHCH or "$CH_2CH + CH_2$". Hence, deep dehydrogenation and decomposition are not an issue on $CuHf_1$, let alone other single-atom alloys which offer weaker stabilization to the surface species. Lastly and most importantly, $CuHf_1$ is much more reactive than the pure Pt catalyst on a per active site basis, and the other two SAA catalysts ($CuIr_1$ and $CuRh_1$) also possess similar propylene production rates to Pt(111). Not only are these Cu-based alloy catalysts much cheaper than the monometallic Pt catalysts for the efficient use of precious metals, but they also attain similar catalytic reactivity and higher selectivity in our modelling. Cu-based dilute alloys could therefore be seen as a versatile and efficient class of catalytic materials for the challenging alkane activation reactions.

Catalyst Stability under Reaction Conditions. Besides catalytic reactivity and selectivity, attention should also be drawn to the stability of the single-atom alloys under high temperature conditions in propane dehydrogenation. Often times, Cu catalysts suffer from sintering at high temperatures, which results in loss of reactivity.[54,55] However, several previous studies have revealed that this situation could be effectively suppressed when a dilute amount of dopant is introduced into Cu.[13,24] In addition to Cu sintering, concern is often raised regarding the surface restructuring (i.e. segregation and aggregation) of the single-atom alloy catalysts, especially in the presence of surface adsorbates and under reaction conditions. Microkinetic modeling indicates that the surfaces of $CuHf_1$ and $CuIr_1$ (Figure 6) are populated by CH_2CHCH_2 and H atoms, respectively, even at high temperature. Due to the adsorbate-dopant bonds, the existence of these surface species can help stabilize the active dopants in the surface layer,[56,57] despite the fact that segregation is a slightly endothermic process for them in the case of the bare surface. To be more specific, the segregation energies (in free energy at T = 773 K) for $CuHf_1$ and $CuIr_1$ become -0.78 eV and -0.72 eV, respectively, in the presence of their corresponding surface adsorbates. Furthermore, one should still attain a significant propylene production rate on $CuHf_1$ even if the reaction temperature is lowered (note that the gaseous species pressures need to be changed accordingly to ensure that the reaction remains exergonic at the reduced temperature) due to the high reaction rates seen in Figure 7. This change in temperature could reduce the energy for the active dopant to diffuse back into the subsurface layer, in addition to minimizing Cu sintering. $CuIr_1$, on the other hand, possesses similar segregation and aggregation energies as $CuRh_1$. In a previous reactor study, it was observed that $CuRh_1$ remains stable for 50 hours during propane dehydrogenation at a reaction temperature of 623 K.[13] Since the strong binding of H atoms on $CuIr_1$, which is not seen in the

case of $CuRh_1$, could help position the active dopants in the surface layer, $CuIr_1$ is expected to demonstrate similar stability at an even higher temperature.

$CuHf_1$ and $CuIr_1$ do not show a tendency to form large active ensembles on the surfaces based on the positive aggregation energies observed in the absence of any adsorbates. Although the presence of surface adsorbates might promote aggregation, this process is proved to be unlikely. DFT calculations demonstrate that the thermodynamic driving force (ΔG) for aggregation to take place in CuHf in the presence of CH_2CHCH_2 is -0.25 eV, while on the bare surface aggregation is unfavorable by 0.56 eV. These two values can be averaged by considering the probability for the dopant to be capped by CH_2CHCH_2, defined as the coverage obtained by the kinetic simulation. The ensemble-average value of the aggregation energy is -0.05 eV at reaction conditions. With such a small magnitude, aggregation could be effectively suppressed by controlling the amount of dopant in Cu. In addition, configurational entropy would further hamper the undesired aggregation. As for CuIr, single H atoms are also shown to be insufficient to markedly bring two surface Ir atoms together, as indicated by the nearly thermoneutral free energy change of 0.01 eV for this process. Despite the fact that our theoretical study suggests Hf and Ir should be able to remain as single atoms in Cu(111), reactor studies are still required to ascertain the stability (and activity) of these alloy catalysts under alkane dehydrogenation conditions.

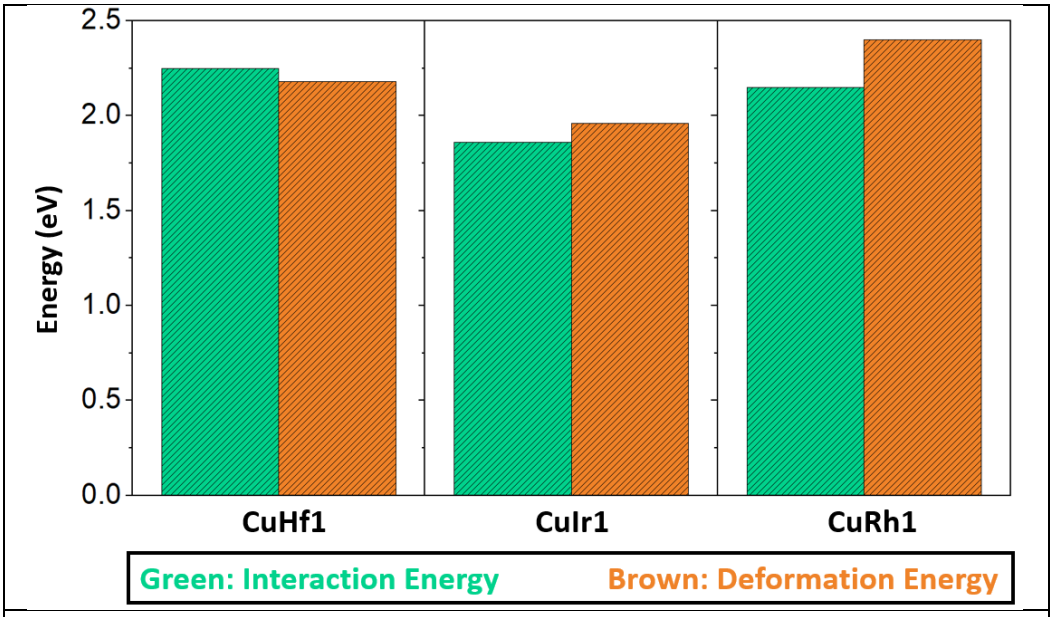

Figure 8. Energy of interaction (absolute value, green) between propane and the surface in the geometry of the transition states for initial C-H bond cleavage, and energy of deformation (brown) of propane in the same transition state geometry.

Origin of Catalytic Activity. The catalytic activity of the single-atom alloys is related to the free energies of the most rate-limiting transition states in the respective more favorable pathways. An energy decomposition scheme,[47] which focuses on the first C-H bond cleavage transition states, was employed to elucidate the magnitude difference. It is understood that on $CuRh_1$, the transition state for H-migration is significantly more rate-controlling than that for C-H bond breaking.

Nevertheless, this study is still useful for the following reasons: (1) these C-H bond breaking transition states themselves play a significant role in controlling the reaction rates (Figure 5), and (2) the free energy of the "CH_3CHCH_3 + H" state, which is the initial state for H-migration on $CuRh_1$, is correlated to the C-H bond breaking transition state based on the Bronsted-Evans-Polanyi relation. To elaborate, the latter indicates that the high intermediate state of "CH_3CHCH_3 + H", which in turn results in the elevated H-migration transition state, can be reflected in the high C-H bond cleavage transition state. From our perspective, an analysis performed in this manner ensures a fair comparison across the single-atom alloy catalysts.

This energy decomposition scheme separates the electronic energy of the transition states into the contributions from the interaction energy between propane and the catalyst surfaces in the constrained geometry of the transition state, and from the distortion energy of propane in that same transition state geometry.[47] It is seen that the interaction energy in the structure of the transition states is the strongest for $CuHf_1$, followed by $CuRh_1$, and $CuIr_1$ (Figure 8). Additionally, $CuHf_1$ is also the only alloy catalyst among the three tested for which the deformation energy of the transition state is lower than the absolute value of the interaction energy. The strong interaction and the relatively small deformation of the transition state on $CuHf_1$ help explain the high reaction activity observed. Although the interaction between the surface species and $CuRh_1$ is much stronger than that with $CuIr_1$, they exhibit rather similar catalytic activity. The reason behind this seeming contradiction is the deformation of the transition state on $CuRh_1$, which is significantly larger than the interaction with the $CuRh_1$ surface. Hence, the positive effect linked with the interaction with $CuRh_1$ is cancelled out. Before wrapping up, it should be noted that the metal slabs are also deformed in the presence of the surface adsorbates. However, their deformation energy magnitudes ($\leq$ 0.15 eV) and the differences among catalysts ($\leq$ 0.04 eV) are small, which make them less useful in the comparison of the transition state free energies.

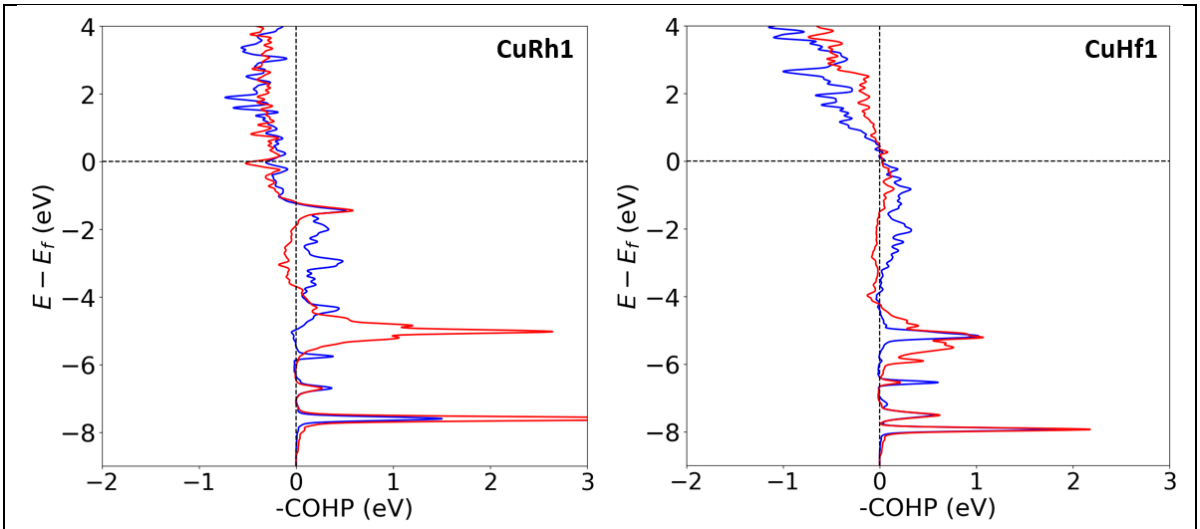

Figure 9. Crystal Orbital Hamilton Population (COHP) for the interactions between the dopants (Hf and Rh) alloyed in Cu(111) and the C (blue) and H (red) atoms in the transition states associated with the first C-H bond cleavage producing CH_3CHCH_3.

A COHP analysis was performed to understand the strong stabilization of the rate-limiting transition state on $CuHf_1$ from a chemical bond perspective (Figure 9). Since the preferred pathway

on $CuHf_1$ and $CuRh_1$ is the same (i.e. forming propylene via CH_3CHCH_3), and the transition states for breaking the first C-H bond in propane adopt similar adsorption configurations on the two surfaces, a COHP curve was also constructed for $CuRh_1$ to enable a comparison. It is worth noting that a portion of the antibonding orbitals (with negative -COHP values) between the Rh dopant and the two atoms (C and H) participating in the bond-breaking step is below the Fermi level (i.e. occupied). This filling of the anti-bonding orbital weakens the interaction between the transition state and the active dopant. Although the anti-bonding orbitals between H and Rh are partially filled, the strong interaction seen for lower energy levels (around 8 eV and 5 eV below Fermi level) can compensate for this destabilization effect. Altogether, the energy integrated ICOHP values for occupied states, characterizing the strength of the bond, are -1.56 between H and Rh and -1.41 between C and Rh. In contrast to $CuRh_1$, the anti-bonding orbitals are seen to be above the Fermi level in almost their entirety for $CuHf_1$, a strengthening factor for the bond between transition state and surface. The more electropositive character of Hf versus Rh pushes the d states towards higher energy, and therefore also the antibonding combination with the adsorbate states. The total ICOHP between Hf and C is -2.16, which is much stronger than in the case of Rh. The ICOHP value between H and Hf, on the other hand, is -1.22; this interaction is somewhat weaker than the case of Rh, from the difference in lower bonding energy states. Altogether, the binding of the rate-limiting transition state as a whole is still stronger on the $CuHf_1$ surface, in line with the lower energy of the transition state and with the higher propylene production rate. This method of diluting different active elements into the Cu metal host can be subsequently seen as an effective approach to shift the position of the anti-bonding orbitals between transition state and surface relative to the Fermi level, and to tune the reactivity for propane dehydrogenation.

Conclusion

DFT calculations and microkinetic modeling have been performed in a synergistic manner to explore dilute alloy catalysts with Cu as a host metal for the propane dehydrogenation reaction. In prior research, $CuRh_1$, where Rh monomers are dispersed in Cu, has been recognized as an active and selective catalyst for that reaction.[13] Our present study extends this knowledge by showing that $CuIr_1$ also exhibits comparable catalytic performance. Surprisingly, C-H bond breaking steps do not exclusively dictate the dehydrogenation rates on these two dilute alloys, contrary to what is typically observed on monometallic catalysts. In addition, the migration by spillover of H atoms away from the dehydrogenated intermediates also plays a pivotal role in controlling the reaction rates, and this is especially true for $CuRh_1$. The possibility of dehydrogenating propyl in the presence of the H atom at the active center was also explored to examine if the rate-limiting H-migration steps can be avoided. Nevertheless, this pathway is demonstrated to be less favorable. Hence, for propane dehydrogenation on single-atom alloys, the steps of species migration on the host metal, in addition to C-H bond activation, also warrant one's attention.

Besides $CuIr_1$, $CuHf_1$ is also predicted to be capable of performing propane dehydrogenation to produce propylene. Compared to $CuIr_1$ and $CuRh_1$, this catalyst is shown to possess a higher rate for propylene formation, despite the fact that some of the active sites are occupied by the dead-end over-dehydrogenated intermediate CH_2CHCH_2. More importantly, its calculated reactivity is even higher than that of the Pt catalyst on a per active site basis, making it an attractive candidate for experimental validation. Our calculations also show that other early-transition metals in Cu(111) (i.e. $CuTi_1$ and $CuZr_1$) will perform similarly to $CuHf_1$ as the rate-determining transition state for propane activation and the most strongly bound intermediate (CH_2CHCH_2) on the three catalysts have comparable free energies.

Within expectation, the low free energy of the rate-limiting transition state and hence the high reaction rate on $CuHf_1$ is attributed to the significant interaction energy between the adsorbate and the surface, which is larger than the transition state deformation energy. COHP analysis further indicates that this strong interaction is a consequence of the depletion of the anti-bonding orbitals between Hf and the two atoms (C and H) participating in the bond-cleavage event of propane. The approach of shifting these anti-bonding orbitals above the Fermi level by dispersing different active elements into the Cu host could hence be used in the rational design of other alloy catalysts for reactive propane dehydrogenation.

Before concluding, it is emphasized that the reactivity of both $CuHf_1$ and $CuIr_1$ is not their sole advantageous attribute. Their intrinsic geometric configurations, characterized by isolated active atoms on the surface, play a pivotal role in mitigating undesired side reactions and inhibiting coke formation − a phenomenon which typically requires larger active ensembles. Consequently, these novel alloy catalysts exhibit remarkable stability and exceptional selectivity for propylene formation. Single-atom alloys could therefore be seen as a promising class of catalytic materials for reactive and selective propane dehydrogenation, and they hold significant potential for advancing current industrial processes.

Acknowledgments

This work was supported as part of the Integrated Mesoscale Architectures for Sustainable Catalysis (IMASC), an Energy Frontier Research Center funded by the U.S. Department of Energy, Office of Science, Basic Energy Sciences under Award No. DE-SC0012573. DFT calculations reported in this work used computational and storage resources on the Hoffman2 cluster at the UCLA Institute for Digital Research and Education (IDRE), the National Energy Research Scientific Computing Center (NERSC) of the U.S. Department of Energy, and the Bridges-2 cluster through the allocation CHE170060 at the Pittsburgh Supercomputing Center through ACCESS.

References

(1) Chen, S.; Chang, X.; Sun, G.; Zhang, T.; Xu, Y.; Wang, Y.; Pei, C.; Gong, J. Propane Dehydrogenation: Catalyst Development, New Chemistry, and Emerging Technologies. *Chem. Soc. Rev.* 2021, *50* (5), 3315–3354.

(2) Ren, Y.; Zhang, F.; Hua, W.; Yue, Y.; Gao, Z. ZnO Supported on High Silica HZSM-5 as New Catalysts for Dehydrogenation of Propane to Propene in the Presence of CO2. *Catal. Today* 2009, *148* (3–4), 316–322.

(3) Baek, J.; Yun, H. J.; Yun, D.; Choi, Y.; Yi, J. Preparation of Highly Dispersed Chromium Oxide Catalysts Supported on Mesoporous Silica for the Oxidative Dehydrogenation of Propane Using CO 2 : Insight into the Nature of Catalytically Active Chromium Sites. *ACS Catal.* 2012, *2* (9), 1893–1903.

(4) Azzam, K. G.; Jacobs, G.; Shafer, W. D.; Davis, B. H. Dehydrogenation of Propane over Pt/KL Catalyst: Investigating the Role of L-Zeolite Structure on Catalyst Performance Using Isotope Labeling. *Appl. Catal. A Gen.* 2010, *390* (1–2), 264–270.

(5) Lavrenov, A. V.; Saifulina, L. F.; Buluchevskii, E. A.; Bogdanets, E. N. Propylene Production Technology: Today and Tomorrow. *Catal. Ind.* 2015, *7* (3), 175–187.

(6) Bhasin, M. M.; McCain, J. H.; Vora, B. V.; Imai, T.; Pujadó, P. R. Dehydrogenation and Oxydehydrogenation of Paraffins to Olefins. *Appl. Catal. A Gen.* 2001, *221* (1–2), 397–419.

(7) Sokolov, S.; Stoyanova, M.; Rodemerck, U.; Linke, D.; Kondratenko, E. V. Comparative Study of Propane Dehydrogenation over V-, Cr-, and Pt-Based Catalysts: Time on-Stream Behavior and Origins of Deactivation. *J. Catal.* 2012, *293*, 67–75.

(8) Yang, M.-L.; Zhu, Y.-A.; Fan, C.; Sui, Z.-J.; Chen, D.; Zhou, X.-G. DFT Study of Propane Dehydrogenation on Pt Catalyst: Effects of Step Sites. *Physical Chemistry Chemical Physics* 2011, *13* (8), 3257.

(9) Im, J.; Choi, M. Physicochemical Stabilization of Pt against Sintering for a Dehydrogenation Catalyst with High Activity, Selectivity, and Durability. *ACS Catal.* 2016, *6* (5), 2819–2826.

(10) Zhu, J.; Yang, M.-L.; Yu, Y.; Zhu, Y.-A.; Sui, Z.-J.; Zhou, X.-G.; Holmen, A.; Chen, D. Size-Dependent Reaction Mechanism and Kinetics for Propane Dehydrogenation over Pt Catalysts. *ACS Catal.* 2015, *5* (11), 6310–6319.

(11) Wang, L.; Wang, L.; Meng, X.; Xiao, F. New Strategies for the Preparation of Sinter-Resistant Metal-Nanoparticle-Based Catalysts. *Advanced Materials* 2019, *31* (50), 1901905.

(12) Sun, S.; Sun, G.; Pei, C.; Zhao, Z.-J.; Gong, J. Origin of Performances of Pt/Cu Single-Atom Alloy Catalysts for Propane Dehydrogenation. *The Journal of Physical Chemistry C* 2021, *125* (34), 18708–18716.

(13) Hannagan, R. T.; Giannakakis, G.; Réocreux, R.; Schumann, J.; Finzel, J.; Wang, Y.; Michaelides, A.; Deshlahra, P.; Christopher, P.; Flytzani-Stephanopoulos, M.; Stamatakis, M.; Sykes, E. C. H. First-Principles Design of a Single-Atom–Alloy Propane Dehydrogenation Catalyst. *Science (1979).* 2021, *372* (6549), 1444–1447.

(14) Han, J.; Lu, J.; Wang, M.; Wang, Y.; Wang, F. Single Atom Alloy Preparation and Applications in Heterogeneous Catalysis. *Chin. J. Chem.* 2019, *37* (9), 977–988.

(15) Giannakakis, G.; Flytzani-Stephanopoulos, M.; Sykes, E. C. H. Single-Atom Alloys as a Reductionist Approach to the Rational Design of Heterogeneous Catalysts. *Acc. Chem. Res.* 2019, *52* (1), 237–247.

(16) Kyriakou, G.; Boucher, M. B.; Jewell, A. D.; Lewis, E. A.; Lawton, T. J.; Baber, A. E.; Tierney, H. L.; Flytzani-Stephanopoulos, M.; Sykes, E. C. H. Isolated Metal Atom Geometries as a Strategy for Selective Heterogeneous Hydrogenations. *Science (1979).* 2012, *335* (6073), 1209–1212.

(17) Darby, M. T.; Stamatakis, M.; Michaelides, A.; Sykes, E. C. H. Lonely Atoms with Special Gifts: Breaking Linear Scaling Relationships in Heterogeneous Catalysis with Single-Atom Alloys. *Journal of Physical Chemistry Letters* 2018, *9* (18), 5636–5646.

(18) Hannagan, R. T.; Giannakakis, G.; Flytzani-Stephanopoulos, M.; Sykes, E. C. H. Single-Atom Alloy Catalysis. *Chem. Rev.* 2020, *120,* 12044-12088.

(19) Ngan, H. T.; Sautet, P. Tuning the Hydrogenation Selectivity of an Unsaturated Aldehyde via Single-Atom Alloy Catalysts. *J. Am. Chem. Soc.* 2024, *146* (4), 2556–2567.

(20) Foucher, A. C.; Ngan, H. T.; Shirman, T.; Filie, A.; Duanmu, K.; Aizenberg, M.; Madix, R. J.; Friend, C. M.; Aizenberg, J.; Sautet, P.; Stach, E. A. Influence of Pd Concentration in Au–Pd Nanoparticles for the Hydrogenation of Alkynes. *ACS Appl. Nano Mater.* 2023, *6* (24), 22927–22938.

(21) Vignola, E.; Steinmann, S. N.; Al Farra, A.; Vandegehuchte, B. D.; Curulla, D.; Sautet, P. Evaluating the Risk of C–C Bond Formation during Selective Hydrogenation of Acetylene on Palladium. *ACS Catal.* 2018, *8* (3), 1662–1671.

(22) Thirumalai, H.; Kitchin, J. R. Investigating the Reactivity of Single Atom Alloys Using Density Functional Theory. *Top. Catal.* 2018, *61* (5–6), 462–474.

(23) Sattler, J. J. H. B.; Ruiz-Martinez, J.; Santillan-Jimenez, E.; Weckhuysen, B. M. Catalytic Dehydrogenation of Light Alkanes on Metals and Metal Oxides. *Chem. Rev.* 2014, *114* (20), 10613–10653.

(24) Shan, J.; Janvelyan, N.; Li, H.; Liu, J.; Egle, T. M.; Ye, J.; Biener, M. M.; Biener, J.; Friend, C. M.; Flytzani-Stephanopoulos, M. Selective Non-Oxidative Dehydrogenation of Ethanol to Acetaldehyde and Hydrogen on Highly Dilute NiCu Alloys. *Appl. Catal. B* 2017, *205*, 541–550.

(25) Zhang, J.; Deng, Y.; Cai, X.; Chen, Y.; Peng, M.; Jia, Z.; Jiang, Z.; Ren, P.; Yao, S.; Xie, J.; Xiao, D.; Wen, X.; Wang, N.; Liu, H.; Ma, D. Tin-Assisted Fully Exposed Platinum Clusters Stabilized on Defect-Rich Graphene for Dehydrogenation Reaction. *ACS Catal.* 2019, *9* (7), 5998–6005.

(26) Zhang, Y.; Zhou, Y.; Shi, J.; Zhou, S.; Sheng, X.; Zhang, Z.; Xiang, S. Comparative Study of Bimetallic Pt-Sn Catalysts Supported on Different Supports for Propane Dehydrogenation. *J. Mol. Catal. A Chem.* 2014, *381*, 138–147.

(27) Zhu, Y.; An, Z.; He, J. Single-Atom and Small-Cluster Pt Induced by Sn (IV) Sites Confined in an LDH Lattice for Catalytic Reforming. *J. Catal.* 2016, *341*, 44–54.

(28) Batzill, M.; Beck, D. E.; Koel, B. E. Electronic Contrast in Scanning Tunneling Microscopy of Sn–Pt(111) Surface Alloys. *Surf. Sci.* 2000, *466* (1–3), L821–L826.

(29) Santhosh Kumar, M.; Chen, D.; Holmen, A.; Walmsley, J. C. Dehydrogenation of Propane over Pt-SBA-15 and Pt-Sn-SBA-15: Effect of Sn on the Dispersion of Pt and Catalytic Behavior. *Catal. Today* 2009, *142* (1–2), 17–23.

(30) Luneau, M.; Shirman, T.; Foucher, A. C.; Duanmu, K.; Verbart, D. M. A.; Sautet, P.; Stach, E. A.; Aizenberg, J.; Madix, R. J.; Friend, C. M. Achieving High Selectivity for Alkyne Hydrogenation at High Conversions with Compositionally Optimized PdAu Nanoparticle Catalysts in Raspberry Colloid-Templated SiO2. *ACS Catal.* 2020, *10* (1), 441–450.

(31) van der Hoeven, J. E. S.; Ngan, H. T.; Yan, G.; Aizenberg, J.; Madix, R. J.; Sautet, P.; Friend, C. M. Unraveling 1-Hexene Hydrogenation over Dilute Pd-in-Au Alloys. *The Journal of Physical Chemistry C* 2022, *126* (37), 15710-15723.

(32) Pei, G. X.; Liu, X. Y.; Wang, A.; Lee, A. F.; Isaacs, M. A.; Li, L.; Pan, X.; Yang, X.; Wang, X.; Tai, Z.; Wilson, K.; Zhang, T. Ag Alloyed Pd Single-Atom Catalysts for Efficient Selective Hydrogenation of Acetylene to Ethylene in Excess Ethylene. *ACS Catal.* 2015, *5* (6), 3717–3725.

(33) Sun, G.; Zhao, Z.-J.; Mu, R.; Zha, S.; Li, L.; Chen, S.; Zang, K.; Luo, J.; Li, Z.; Purdy, S. C.; Kropf, A. J.; Miller, J. T.; Zeng, L.; Gong, J. Breaking the Scaling Relationship via Thermally Stable Pt/Cu Single Atom Alloys for Catalytic Dehydrogenation. *Nat. Commun.* 2018, *9* (1), 4454.

(34) Zha, S.; Sun, G.; Wu, T.; Zhao, J.; Zhao, Z.-J.; Gong, J. Identification of Pt-Based Catalysts for Propane Dehydrogenation *via* a Probability Analysis. *Chem. Sci.* 2018, *9* (16), 3925–3931.

(35) Kresse, G.; Hafner, J. Ab Initio Molecular Dynamics for Liquid Metals. *Phys. Rev. B* 1993, *47* (1), 558–561.

(36) Kresse, G.; Hafner, J. Ab Initio Molecular-Dynamics Simulation of the Liquid-Metalamorphous- Semiconductor Transition in Germanium. *Phys. Rev. B* 1994, *49* (20), 14251–14269.

(37) Gautier, S.; Steinmann, S. N.; Michel, C.; Fleurat-Lessard, P.; Sautet, P. Molecular Adsorption at Pt(111). How Accurate Are DFT Functionals? *Physical Chemistry Chemical Physics* 2015, *17* (43), 28921–28930.

(38) Dion, M.; Rydberg, H.; Schröder, E.; Langreth, D. C.; Lundqvist, B. I. Van Der Waals Density Functional for General Geometries. *Phys. Rev. Lett.* 2004, *92* (24), 246401.

(39) Román-Pérez, G.; Soler, J. M. Efficient Implementation of a van Der Waals Density Functional: Application to Double-Wall Carbon Nanotubes. *Phys. Rev. Lett.* 2009, *103* (9), 096102.

(40) Klimeš, J.; Bowler, D. R.; Michaelides, A. Chemical Accuracy for the van Der Waals Density Functional. *Journal of Physics: Condensed Matter* 2010, *22* (2), 022201.

(41) Pulay, P. Convergence Acceleration of Iterative Sequences. the Case of Scf Iteration. *Chem. Phys. Lett.* 1980, *73* (2), 393–398.

(42) Henkelman, G.; Jónsson, H. Improved Tangent Estimate in the Nudged Elastic Band Method for Finding Minimum Energy Paths and Saddle Points. *J. Chem. Phys.* 2000, *113* (22), 9978–9985.

(43) Henkelman, G.; Uberuaga, B. P.; Jónsson, H. Climbing Image Nudged Elastic Band Method for Finding Saddle Points and Minimum Energy Paths. *Journal of Chemical Physics* 2000, *113* (22), 9901-9904.

(44) Henkelman, G.; Jónsson, H. A Dimer Method for Finding Saddle Points on High Dimensional Potential Surfaces Using Only First Derivatives. *Journal of Chemical Physics* 1999, *111* (15), 7010–7022.

(45) Maintz, S.; Deringer, V. L.; Tchougréeff, A. L.; Dronskowski, R. LOBSTER: A Tool to Extract Chemical Bonding from Plane-Wave Based DFT. *J. Comput. Chem.* 2016, *37* (11), 1030–1035.

(46) Momma, K.; Izumi, F. VESTA 3 for Three-Dimensional Visualization of Crystal, Volumetric and Morphology Data. *J. Appl. Crystallogr.* 2011, *44*, 1272-1276.

(47) VALERO, M.; RAYBAUD, P.; SAUTET, P. Interplay between Molecular Adsorption and Metal–Support Interaction for Small Supported Metal Clusters: CO and C2H4 Adsorption on Pd4/ΓPd4/γ-Al2O3. *J. Catal.* 2007, *247* (2), 339–355.

(48) Gokhale, A. A.; Kandoi, S.; Greeley, J. P.; Mavrikakis, M.; Dumesic, J. A. Molecular-Level Descriptions of Surface Chemistry in Kinetic Models Using Density Functional Theory. *Chem. Eng. Sci.* 2004, *59* (22–23), 4679–4691.

(49) Campbell, C. T. The Degree of Rate Control: A Powerful Tool for Catalysis Research. *ACS Catal.* 2017, *7* (4), 2770–2779.

(50) Al-Douri, A.; Sengupta, D.; El-Halwagi, M. M. Shale Gas Monetization – A Review of Downstream Processing to Chemicals and Fuels. *J. Nat. Gas Sci. Eng.* 2017, *45*, 436–455.

(51) Shi, J.; Owen, C. J.; Ngan, H. T.; Qin, S.; Mehar, V.; Sautet, P.; Weaver, J. F. Formation of a Ti–Cu(111) Single Atom Alloy: Structure and CO Binding. *J. Chem. Phys.* 2021, *154* (23), 234703.

(52) Lee, J. D.; Qi, Z.; Foucher, A. C.; Ngan, H. T.; Dennis, K.; Cui, J.; Sadykov, I. I.; Crumlin, E. J.; Sautet, P.; Stach, E. A.; Friend, C. M.; Madix, R. J.; Biener, J. Facilitating Hydrogen Dissociation over Dilute Nanoporous Ti–Cu Catalysts. *J. Am. Chem. Soc.* 2022, *144* (37), 16778-16791.

(53) Hanh, T. T. T.; Takimoto, Y.; Sugino, O. First-Principles Thermodynamic Description of Hydrogen Electroadsorption on the Pt(111) Surface. *Surf. Sci.* 2014, *625*, 104–111.

(54) Twigg, M. V.; Spencer, M. S. Deactivation of Supported Copper Metal Catalysts for Hydrogenation Reactions. *Appl. Catal. A Gen.* 2001, *212* (1–2), 161–174.

(55) Twigg, M. V.; Spencer, M. S. Deactivation of Copper Metal Catalysts for Methanol Decomposition, Methanol Steam Reforming and Methanol Synthesis. *Top. Catal.* 2003, *22*, 191–203.

(56) Fu, Q.; Luo, Y. Catalytic Activity of Single Transition-Metal Atom Doped in Cu(111) Surface for Heterogeneous Hydrogenation. *The Journal of Physical Chemistry C* 2013, *117* (28), 14618–14624.

(57) Darby, M. T.; Sykes, E. C. H.; Michaelides, A.; Stamatakis, M. Carbon Monoxide Poisoning Resistance and Structural Stability of Single Atom Alloys. *Top. Catal.* 2018, *61* (5–6), 428–438.

TOC

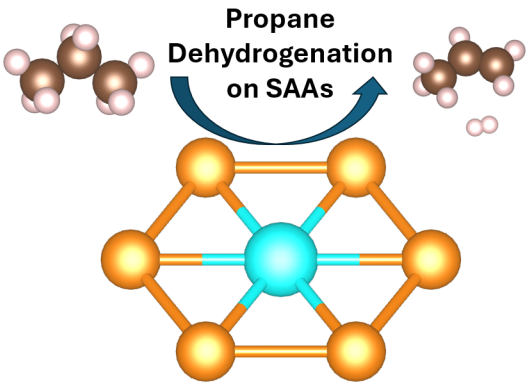

CuHf1 > Pt(111) > CuIr1 and CuRh1
Propylene Formation Rate